LIMITATIONS AND EXTENSIONS OF THE MAKISHIMA MACKENZIE MODEL

by

Michał Plucinski

Submitted in partial fulfillment of the
requirements for the degree of
Masters of Science

at

Dalhousie University
Halifax, Nova Scotia
September 2014

Table of Contents

List of Tables

List of Figures

Abstract

The Makishima Mackenzie model, used to predict the elastic properties of glass, is explored in terms of both accuracy and predictive properties. Its limitations are outlined, in particular for borate glass, and a new framework is proposed to explain the mechanics that underlie the elasticity of network systems. This framework explains the limitations of the Makishima Mackenzie model, and why it functions in many but not all cases. The overall level of rigidity of the system can be predicted with the counts of the number of constraints and degrees of freedom in a system.

Simulations are also performed that explore the dependency of elastic properties on various variables. The density of a system is found to be independent of elasticity, while the average coordination number is found to be strongly dependent. A new equation is determined that connects the Young's modulus and the average coordination number, applicable for constrained systems.

List of Abbreviations and Symbols Used

A	Area
B	Bulk modulus
C	Undefined constant
E	Young's modulus
E_b	Bond energy
F	Force
G	Dissociation energy
L	Length
M	Effective molecular weight
N_c	Number of constraints
N_d	Number of degrees of freedom
P	Pressure
R	Ionic radius
S	Rigidity modulus
U	Potential Energy
U_i	Internal Energy
V	Rigidity modulus
V_t	Packing density
W	Work
X	Mole fraction
$\langle r \rangle$	Average coordination number
ρ	Density
σ	Stress

ε	Strain
c	Elastic tensor
e	Ion charge
k	Elastic stiffness constant in Hooke's Law
r_0	Interatomic distance
s	Compliance tensor

MM model	Makishima Mackenzie model

Acknowledgements

First and foremost, I'd like to thank Dr. Josef Zwanziger for all the lessons he has taught me, and his invaluable guidance.

Dr. Russell Boyd and Dr. Peng Zhang gave me much appreciated advice as members of my committee, and they have my gratitude.

Many thanks to my whole lab group for their help in answering questions and exploring the key ideas in my thesis: Courtney Calahoo, Justine Galbraith, Alex Paterson, Dr. Saumitra Saha, Dr. Gao Tang, Jeremy Thorbahn, Dr. Tsanka Todorova, and Dr. Margaret Hanson.

I'd also like to thank Dr. Axel Kohlmeyer from Temple University, for helping me learn the functions and subtleties of LAMMPS.

Finally, last but not least, my family and friends have been incredible in their support over these last two years working on this thesis.

Chapter 1

Introduction

The elastic properties of materials describe how they respond to small deformations - deformations that do not fracture the material and allow it to return to its original state once the deformation is no longer applied (1). Material requirements for various applications differ greatly, from very stiff to compliant. In order to create a new material that has a desired elasticity, it is necessary to understand how elastic properties arise and to be able to predict them. A good understanding of how varying the chemical composition will make the process of selecting a new material more efficient by narrowing the choice to the most promising of potential materials (2).

Glass in particular is an exciting field of research, with many different possible applications, from smartphone covers, to fibre optic networks, to basic window glass. Each of these applications require different elastic properties, and so different types glass are used for them. The importance of methods to connect the macroscopic properties of glass to the chemical structure was outlined in a paper from Corning Incorporated in 2014 (2) which states, "It is ... critical to conduct fundamental research to develop a detailed understanding of the composition ... dependence of glass structure and its relationship to macroscopic properties." This fundamental research will build on the model that was outlined in the 1970s by A. Makishima and J. D. Mackenzie (3) that aims to predict the elastic properties of oxide glasses based on the structural properties of their component crystal oxides.

The glasses considered in this study, and indeed most types of glass, are composed of different oxide crystals combined at high temperatures. Crystals have long range

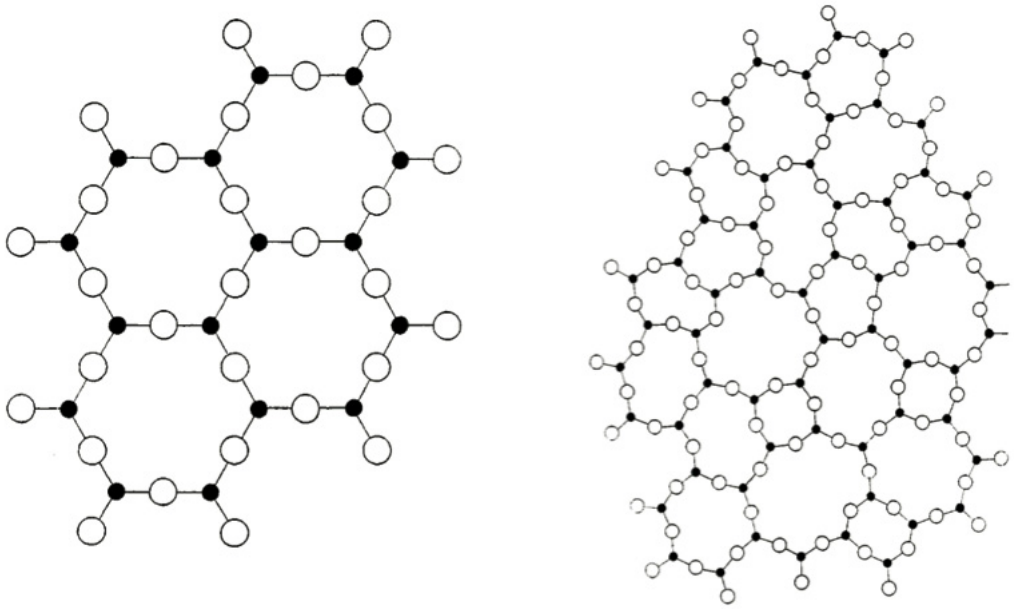

Figure 1.1: The Difference Between a Glass and a Crystal. Figure reproduced from reference (4).

order, and are made up of repeating units throughout the whole material. In contrast, glass has no long range order. However, it shares its short range order with the crystals it is made up of, and has the same basic chemical units as in a crystal. The difference is that there is no order in how those units are arranged over long distances. This difference is illustrated in figure 1.1. In the case of SiO_2, the silicon atoms are bonded to four oxygen atoms in a tetrahedral coordination, and each oxygen atom is bonded to two silicon atoms in a bent coordination. The chemical bonding properties are very similar in both the glass and the crystal, so the properties of the crystal should be correlated with the properties of the glass.

Indeed, the Makishima Mackenzie model uses the properties of the component crystals that are used to create a glass to predict its properties. To be able to make this prediction, the model must develop a way to account for the lack of long range order in glass - long range order that is present in the crystal. The model works rather well for many different types of glass, but unfortunately fails quite badly for

glasses made from B_2O_3, as outlined in the original Makishima Mackenzie paper. Its successes and failures are a result of its description of how elastic properties are related to the underlying structure of the glass. It posits that glass is made up of a series of units defined by the coordination centres (Silicon and Oxygen in the case of silicate glass) and assumes these centres interact as a group of elastic balls, with their stiffness defined by their bond dissociation energy. The bond dissociation energy used was determined using the methods created by Sun and Huggins in 1946 (5).

Makishima and Mackenzie's model has been used frequently to predict the elastic properties of glasses, with over one hundred citations. It was originally derived for the Young's modulus, but later extended to calculations of the other elastic properties (6). There are numerous examples of the MM model being used to confirm experimental measurements in a large variety of systems: phosphate glasses (7), borate glasses (8; 9; 10), and silicate glasses (11), with various different components in the glass. The researchers in all these cases used the key elements of the MM model to make arguments about the underlying structural properties of the glasses tested.

However, if there are problems with the model, making structural arguments on its basis may be problematic. For example, for borate glasses, the researchers generated their theoretical predictions using a correction proposed by Makishima and Mackenzie in their original paper (8; 9; 10). Huang's et al. DFT and MD calculations give reason to dispute the validity of this correction (12; 13).

Additionally, the model is found to fail in a number of papers, not matching experimental properties well: some papers showed predicted values far from those calculated by the MM model (14; 15), others had success for only specific compositions and not across a glass series (16). These failures suggest some limitations of the model, and others have attempted to improve the model to avoid similar failures. In a paper on "Elastic Properties and Short-to Medium-Range Order in Glasses" in the Journal of the American Ceramics Society, Rouxel outlines the assumptions of the

MM model, and questions in particular a logical leap the model makes from crystal to glass structure (17). This question will be considered in more detail below. In another piece for the same journal, Inaba et al. (18) suggest improving the model by refining the data input, but do not question any of the model's underlying assumptions. These result in empirical improvements to the predictions of the model for specific systems.

Applications of empirical improvements however are unsatisfactory, as the dramatic failure of the model for borate glass suggests that there may be more fundamental issues. Thorpe (19) suggests a connection between elastic properties and bond order. His paper in The Journal of Non-Crystalline Solids outlines the concept of percolation and suggests a new one of rigidity percolation. Rigidity percolation explains how the elastic properties of network systems depend on the connectivity in the system. The model system studied by Thorpe was a simple one, as outlined in a concurrent paper (20), with two-body Hookean springs representing bonds between atoms, and no other forces present. Interestingly, the paper found that the c_{11} elastic constant decreased to zero at an average coordination number of 2.4 for the system, the same coordination found in borate glasses. This suggests a connection between the average coordination number and elastic properties in a system.

The paper by Thorpe was expanded upon significantly in a later paper by Boolchand, Lucovsky, Phillips, and Thorpe (21). This work built on the original Thorpe paper by adding three-body potentials to its analysis to be able to examine elastic properties other than just c_{11}. More importantly however, it added a new model for understanding the rigidity of network systems, based on a comparison of the numbers of constraints and degrees of freedom present in a system. This would explain why the elasticity of network systems is related to the average coordination number of the bonding centres. An increased bonding in the system would increase the number of constraints, and thus the rigidity of the system, while a decrease would cause the

opposite (or even cause the system to collapse). The principles of this model of rigidity explains the relationship of rigidity to the average coordination observed in the experiments below, and suggest how the MM model might be improved.

The next chapters will develop a series of computations to test a more advanced model of network materials, i.e. glasses and crystals, for the calculation of elastic properties. They will examine how different microscopic and macroscopic properties affect the elastic properties of the material, and show which ones are the most important to include in a predictive model. In the course of this examination, it will be revealed that the Makishima Mackenzie model mistakenly accounts for certain factors, while ignoring others. In its place, the author proposes a new model, the constraints model, which explains why the MM model works for certain glasses, but not others. Based on this model, one can develop an equation that better includes the properties most important to predicting elasticity. This equation is then applied to systems previously studied by the MM model. Based on these results, the author proposes a pathway forward to develop a more comprehensive model for predicting the elasticity of glasses.

Chapter 2

Theory

In this chapter, the background theory underlying the methods used throughout this thesis will be explained. First the bulk modulus will be calculated for a six-coordinated mono-atomic periodic system, with bonds defined as Hookean springs. This computation will introduce basic concepts and provide an example of how to solve for an elastic property of a simple system. Next the methods used to solve larger and more complex problems will be outlined - these are the methods used to calculate elastic properties for the models in this work. These predicted elastic constants will be connected to actual experimental parameters, and the estimations and assumptions made in this connection will be outlined. Finally, the Makishima Mackenzie model will be presented.

2.1 Solving a Mono-Atomic Periodic Hooke Spring System

To begin, the bulk modulus is defined, then the model system to be solved is described, and finally the bulk modulus is computed for this system.

2.1.1 Bulk modulus

The bulk modulus describes the resistance of a substance to uniform compression. It is defined as:

$$B = -V \left(\frac{\partial P}{\partial V} \right)_T , \tag{2.1}$$

where V is the volume of the system, P is its internal pressure, and T is its temperature. However, to facilitate calculation in a simulation model, the bulk modulus must be expressed in terms of potential energy, not pressure. So, pressure is defined in terms of internal energy, U_i:

$$P = -\left(\frac{\partial U_i}{\partial V}\right)_S, \tag{2.2}$$

where S is the entropy of the system. Substituting 2.2 into 2.1 gives

$$B = V\left(\frac{\partial^2 U_i}{\partial V^2}\right)_{T,S}. \tag{2.3}$$

Now the bulk modulus is defined in terms of variables which can be solved for directly. Temperature and entropy must be kept constant for this definition to be correct.

2.1.2 The Model System

The system under study is represented by a cell. The cell is primitive cubic, with unit side lengths, and therefore a unit volume. It is a periodic cell, so it represents a system that repeats to infinity in each axis. The unit cell contains a single atom, supposed to be at the corner. Each atom is six-fold coordinate, with unit bonds lengths. This is illustrated in figure 2.1.

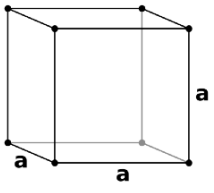

Bond Length $= a = 1$ $\quad V = a^3 = 1^3$

Figure 2.1: The unit cell of the model system (1)

Because B is defined in terms of the change in the potential with respect to changes in volume, the volume of the cell will need to be varied. To do this, each side length

is dilated by x, which is equal in every direction. This also changes the definitions of the bond lengths in the cell and of the volume, as shown in figure 2.2.

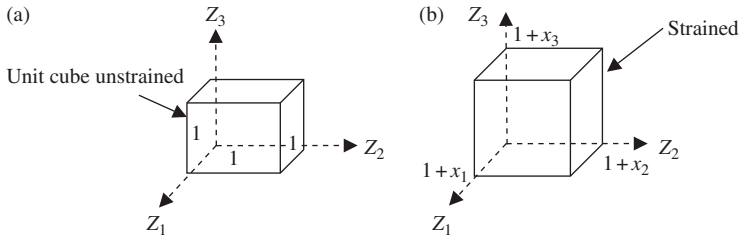

Bond Length $= (1 + x)$ $\quad V = (1 + x)^3$

Figure 2.2: The perturbed unit cell of the model system (1)

In this system, varying x will not vary the temperature or entropy of the system, allowing the equation for bulk modulus previously defined to be used. This is due to the fact that the temperature remains at zero kelvin for the system at all times, and the number of states remains fixed when changing the volume of the system.

2.1.3 The Potential

As previously stated, this is to be a Hooke spring system, so every bond will be a Hooke spring, with potential energy

$$u = \tfrac{1}{2}kd^2, \tag{2.4}$$

where k is the spring constant and d is the bond length. Here, the potential is zero at $d = 0$, but the energy ought to be zero at the unperturbed state of the model, or where $x = 0$ and $d = 1$. So the zero of the potential is shifted:

$$u = \tfrac{1}{2}kd^2 \rightarrow u = \tfrac{1}{2}k(d-1)^2. \tag{2.5}$$

The effect of this potential shift is represented in figure 2.3.

Now to find the total energy of the system, the potentials of all the bonds are added together:

$$U = \frac{1}{2} \sum_{<i,j>} \frac{1}{2} k(d_{ij} - 1)^2, \tag{2.6}$$

where d_{ij} is the distance from atom i to j, the sum is over nearest-neighbour pairs, and the additional factor of $\frac{1}{2}$ avoids double counting of pairs.

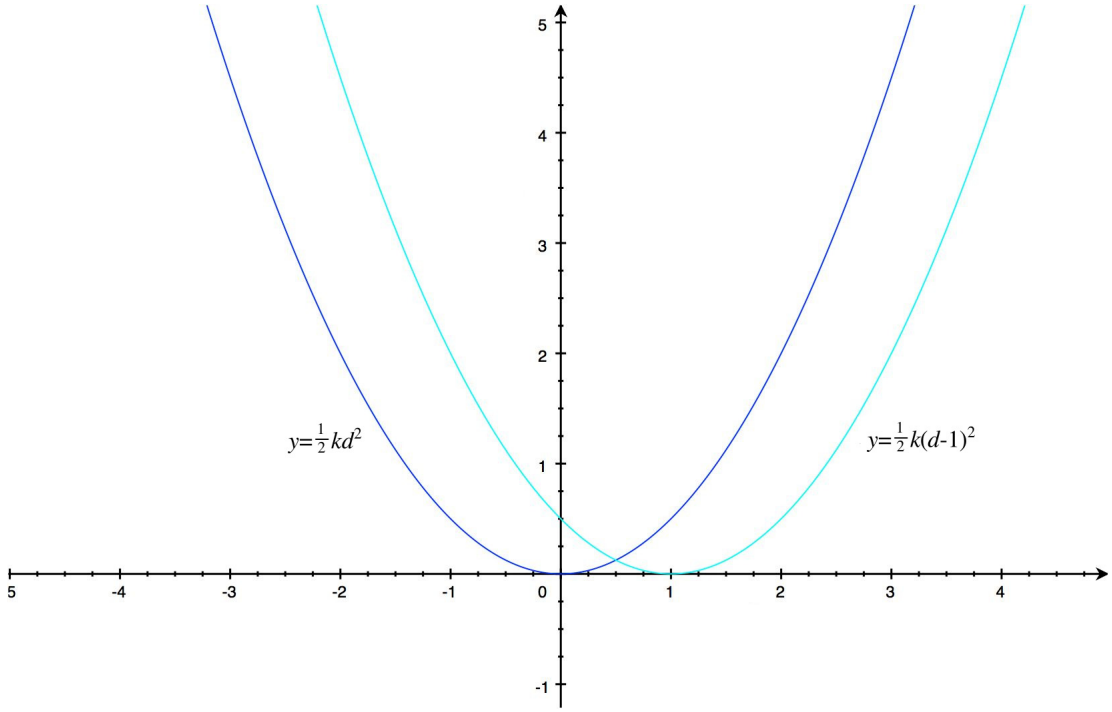

Figure 2.3: Shifting a harmonic potential to represent a zero-energy bond length

The energy per unit cell is simply

$$U = 3 \cdot \frac{1}{2} k(d - 1)^2, \tag{2.7}$$

as there is a single atom with 6 bonds.

2.1.4 The Solution

Although the bulk modulus was defined in terms of internal energy, because this is a classical system without any quantum effects, and because the temperature is set to 0 K, the internal energy is equal to the potential energy of the system. Thus, the bulk modulus can be defined by equation 2.3.

To compute the bulk modulus, d is substituted with the bond length, $1 + x$,

$$U = \tfrac{3}{2}kx^2. \tag{2.8}$$

If the system is unperturbed, at $x = 0$, the total energy is zero. Next, the potential is redefined in terms of the volume, so the equation for bulk modulus can be used:

$$V = (1 + x)^3 \rightarrow x = V^{1/3} - 1,$$

$$\therefore U = \tfrac{3}{2}k(V^{1/3} - 1)^2. \tag{2.9}$$

In the series expansion of equation 2.9 around the energy minimum, $V = 1$, the first term has a coefficient of $\frac{1}{6}$, while the second term has the much lower coefficient of $\frac{1}{54}$. To find the bulk modulus of a system with a volume of one, only minor perturbations need to be made. With small perturbations, the first term dominates and higher order terms need not be considered. This limitation of small perturbations would apply to solutions for much larger and more complex systems as well: these systems can only be considered to be symmetric in positive or negative compression if the perturbations are small relative to their size of the system. In the series expansion, the linear order term vanishes, and the first non-zero term is the quadratic term. It is good that the linear order term vanishes, as with a coefficient of $\frac{3}{2}$, it would have a dominant effect on the system, and the potential would no longer be symmetric around the energy minimum of the system.

$$\text{at } V = 1,$$

$$U \doteq \tfrac{1}{6}k(V-1)^2. \tag{2.10}$$

Finally, the derivative solves for the bulk modulus:

$$B = -V_0\left(\frac{\partial^2 U}{\partial V^2}\right) = \tfrac{1}{3}k \cdot V_0. \tag{2.11}$$

2.2 Calculation of Elastic Properties for Complex Systems

2.2.1 Stress, Strain, and the Elastic Tensor

The elastic properties of solids describe how solids react to the deformations of stress and strain. To measure an elastic property, one must apply a specific stress or strain to the system. Stress is defined as the force per unit area on a solid, while strain is change in length per unit length:

$$\sigma = F/A, \tag{2.12}$$

$$\varepsilon = \Delta L/L, \tag{2.13}$$

where ε is the strain, L is the length of the system, ΔL the change in length, σ is the stress, F is force, and A is area.

Define σ_{ij} to be a stress tensor and ε_{ij} to be a strain tensor. These are both 6x6 tensors that define the way the deformation is applied to the system. Each individual element of the tensor defines magnitude this deformation in a particular direction, which makes the values of the elements interdependent. For stress, σ_{xz} would be the magnitude of force in the x direction over the area of the face normal to z. Thanks

to the interdependence of elements, this is equal to ε_{zx}. For strain, ε_{ij} would equal to the magnitude of internal length change in the x direction over the length of z. Remember that if σ_{xz} is non-zero, so are σ_{zx}, σ_{xx}, and σ_{zz}.

For very small stresses and strains, the influence of these two different types of deformations is related by the elastic tensor defined by Hooke's Law. Hooke's Law assumes that the deformation of the system is linear with respect to the applied stress. Linearity means that each stress component is linearly related to the strains, through the following equation:

$$\sigma_{ij} = c_{ijkl}\varepsilon_{kl}, \tag{2.14}$$

where sums over repeated indices are implied.

As ε_{ij} and σ_{kl} are 2nd order tensors with 9 elements each, c_{ijkl} is a 4th order tensor with 81 elements This is called the elastic stiffness tensor. However, since the strain and stress are symmetric tensors with only 6 independent elements each, the number of independent elements of c can be reduced to 36 elements.(1)

$$\begin{pmatrix}\sigma_1\\ \sigma_2\\ \sigma_3\\ \sigma_4\\ \sigma_5\\ \sigma_6\end{pmatrix} = \begin{pmatrix}c_{11} & c_{12} & c_{13} & c_{14} & c_{15} & c_{16}\\ c_{21} & c_{22} & c_{23} & c_{24} & c_{25} & c_{26}\\ c_{31} & c_{32} & c_{33} & c_{34} & c_{35} & c_{36}\\ c_{41} & c_{42} & c_{43} & c_{44} & c_{45} & c_{46}\\ c_{51} & c_{52} & c_{53} & c_{54} & c_{55} & c_{56}\\ c_{61} & c_{62} & c_{63} & c_{64} & c_{65} & c_{66}\end{pmatrix}\begin{pmatrix}\varepsilon_1\\ \varepsilon_2\\ \varepsilon_3\\ \varepsilon_4\\ \varepsilon_5\\ \varepsilon_6\end{pmatrix} \tag{2.15}$$

In the above matrix, the indices for each element are defined by Voigt notation, which takes the symmetry of the tensors into account and means the tensors no longer need to be expressed in terms of all $ijkl$, but in terms of ij where $ij \rightarrow i$ and $kl \rightarrow j$. In Voigt notation, the directions xx, yy, zz, yz, xz, xy are defined as 1, 2, 3, 4, 5, 6.

The inverse relationship between strain and stress defines the compliance tensor, the inverse of the stiffness tensor:

$$\varepsilon_i = (c_{ij})^{-1}\sigma_j = s_{ij}\sigma_j. \tag{2.16}$$

2.2.2 Relation to Potential Energy

To solve for the tensor elements, the tensor elements (or elastic constants) must be defined in terms of potential energy, as potential energy is what theoretical models calculate. The product of stress and strain turns out to be the stored mechanical energy density:(1)

$$\partial W = \sigma_i \partial \varepsilon_i = c_{ij} \varepsilon_j \partial \varepsilon_i, \tag{2.17}$$

where W is work. Since applying small strains that satisfy Hooke's law is an approximately adiabatic process, this relationship can be redefined in terms of potential energy, using the first law of thermodynamics,

$$\frac{\partial U}{\partial \varepsilon_i} = \sigma_i = c_{ij} \varepsilon_j. \tag{2.18}$$

Taking the second derivative solves for c:

$$\frac{\partial U}{\partial \varepsilon_i \partial \varepsilon_j} = \frac{\partial \sigma_i}{\partial \varepsilon_j} = c_{ij}. \tag{2.19}$$

These formula are conveniently defined as derivatives in terms of changes in the strain tensor. This is useful, as it is computationally more straightforward to apply an internal deformation of the whole system than it is to apply an outside force. Thus, a computation of total energy can be used to obtain the elastic constants.

Alternatively, if stress are available, the second part of equation 2.19 can be used:

$$\frac{\partial \sigma_i}{\partial \varepsilon_j} = c_{ij}.$$

As previously stated, the stress tensor is defined as $\sigma_{ij} = F_i / A_j$. This is conveniently

also the definition of the local pressure tensor(22) $p_{ij} = F_i/A_j$. The effect on the stress from the changes in strain can be measured to get the elastic constants.

2.3 Predicting Experimental Elastic Constants from Theoretical Calculations

It has been demonstrated how to calculate an elastic property for a simple theoretical model, and how to calculate the entire elastic tensor from the potential energy of any solid. The connection must to be drawn from these calculated constants back to experimentally determined elastic constants. Two key elastic constants will be considered: the rigidity modulus S and bulk modulus B. Calculate these may be calculated from either the strain tensor c or the compliance tensor s. Two averaging methods, the Voigt and Reuss methods (23; 24), define these three constants from the two tensors in different ways.

$$S_V = \tfrac{1}{15}(c_{11} + c_{22} + c_{33}) - (c_{12} + c_{23} + c_{31}) + 3(c_{44} + c_{55} + c_{66}) \tag{2.20}$$

$$B_V = \tfrac{1}{9}(c_{11} + c_{22} + c_{33}) + 2(c_{12} + c_{23} + c_{31}) \tag{2.21}$$

$$\frac{15}{S_R} = 4(s_{11} + s_{22} + s_{33}) - 4(s_{12} + s_{23} + s31) + 3(s_{44} + s_{55} + s_{66}) \tag{2.22}$$

$$\frac{1}{B_R} = (s_{11} + s_{22} + s_{33}) + 2(s_{12} + s_{23} + s_{31}) \tag{2.23}$$

Here S_V is the Voigt average for S, S_R is the Reuss average; B_V is the Voigt average for B, B_R is the Reuss average. The Voigt averaging method performs the calculation from c, assuming uniform strain, while the Reuss averaging method assumes uniform stress and thus uses s. This means that neither of these averages match the true experimental conditions; there are bound to be variations in stress and strain throughout the sample. But there is one exception for cubic cells: bulk modulus. Since measuring

bulk modulus involves only an isotropic volume change, the stress and strain can be assumed to be both uniformly distributed. From the above formula 2.21 and 2.23,

$$B_R = B_V = \tfrac{1}{3}(c_{11} + 2c_{12}). \tag{2.24}$$

For calculations of the rigidity modulus, as well as other moduli, a further average must be made to get a reasonable approximation of true experimental values: the Voigt-Reuss-Hill approximation (25). As both Voigt and Reuss methods assume an opposite extreme, the average of the two of them is used to predict realistic experimental elastic constants:

$$S = \tfrac{1}{2}(S_V + S_R). \tag{2.25}$$

And so, it has been demonstrated how to solve for the bulk modulus in a simple repeating lattice, how to generally calculate the elastic tensor for any solid from its potential energy, and finally how to use these tensor elements to calculate experimental elastic properties. In the following chapters, these core theories are applied to form the basis for the work of this thesis.

2.4 The Makishima Mackenzie Model

Before the aforementioned theories are applied, the theory of the model that motivates this work must first be outlined: the Makishima Mackenzie model. The MM model was introduced in a paper published in the Journal of Non-Crystalline Solids in 1973 by A. Makishima and J. D. Mackenzie. (3) The model estimates the elastic properties of glass using the atomic properties of their component oxides in crystal form as input variables. This model works reasonably well for predicting the elastic properties of a wide variety of glasses with different component oxides, but unfortunately does not generate very good predictions for boron oxide glasses. The derivation of the model for

determining the Young's modulus of glass, the implications of the derived equations, and the assumptions behind them will be outlined. Then, the model's failure for borate glasses will be shown, followed by the proposed correction to the model for this failure, as described in the original paper.

2.4.1 Derivation

To begin the derivation of the Makishima Mackenzie model, the Young's modulus (E) for an ionic crystal is derived. So, the electrostatic energy of attraction, U, is defined for a pair of ions with opposite sign:

$$U = -e^2/r_0, \tag{2.26}$$

where e is the charge of the ions, and r_0 is the distance between the ions. Next, this energy is multiplied by the Madelung constant α to account for the many ionic interactions within a crystal, giving the Madelung energy, U_m:

$$U_m = \alpha U. \tag{2.27}$$

Remembering the definition of stress in equation 2.12, and using the fact that the force between ions is $\partial U_m/\partial r$, the stress σ is

$$\sigma = \frac{1}{r_0^2}\left(\frac{\partial U_m}{\partial r}\right). \tag{2.28}$$

The change of stress for a change in r is $d\sigma/dr$,

$$d\sigma = \frac{dr}{r_0^2}\left(\frac{\partial^2 U_m}{\partial r^2}\right). \tag{2.29}$$

This is equal to $Ed\varepsilon$, according to the definition of $E = \frac{d\sigma}{d\varepsilon}$, where the strain $d\varepsilon = dr/r_0$, as previously defined in equation 2.13. Therefore,

$$E = \frac{d\sigma}{d\varepsilon} = \frac{1}{r_0}\left(\frac{\partial^2 U_m}{\partial r^2}\right) = \frac{2\alpha e^2}{r_0^4}. \tag{2.30}$$

This inverse relationship to r_0^4 has been experimentally confirmed. Thus, the Young's modulus for ionic crystals can be defined in terms of their energy of attraction and interatomic spacing:

$$E = \frac{2\alpha}{r_0^3}\left(\frac{e^2}{r_0}\right) = 2\frac{U\alpha}{r_0^3}. \tag{2.31}$$

The working assumption so far has been for a system of ionic crystals. However, for oxide glasses, a Madelung constant can no longer be adopted as the system has no long range order. Therefore, U_m/r_0^3 is replaced by the product of dissociation energy per unit volume, G, and the packing density of ions, V_t. This is the critical point where the MM models makes its leap from a system with long range order to one with only short range order. The volumetric dissociation energy is a substitute for the whole term. However the dissociation energy is calculated per volume of the whole cell, while equation 2.31 is defined in terms of the ionic volume. The packing density V_t corrects for this difference, giving the key MM model equation,

$$E = 2GV_t. \tag{2.32}$$

For polycomponent glasses,

$$E = 2V_t \sum_i G_i X_i, \tag{2.33}$$

$$V_t = \frac{\rho}{M} \sum_i V_i X_i, \tag{2.34}$$

where M is the effective molecular weight and ρ is the density of the glass, X_i is the mole fraction of component i, and V_i is the packing factor obtained for an oxide

$A_X O_Y$:

$$V_i = 6.023 \times 10^{23} \frac{4}{3} \pi (X R_A^3 + Y R_O^3), \tag{2.35}$$

with R_A and R_O the respective ionic radii of the metal and oxygen. The packing fraction can be thought of as the proportion of space filled in the cell by spheres around the atoms. The radii of these spheres is defined by their ionic radii. A totally full cell would give $V_t = 1$ and an absence of atoms would have $V_t = 0$.

$E = 2GV_t$ is the form that will be returned to later in this thesis, as working with poly-component glasses would only complicate the analysis.

For the purposes of the model, neither the interatomic spacing nor the bonding strength is assumed to change between the ionic oxide crystal that makes up the glass, and for the properties of the glass itself. Also, the atoms are assumed to interact as spherical ions in both the crystal and the glass. Therefore, the model can be thought of as representative of a set of ionic balls whose repulsive strength is defined by the dissociation energy per volume of the glass. This is illustrated for a crystal in figure 2.4, and the MM model applies this metaphor to glass.

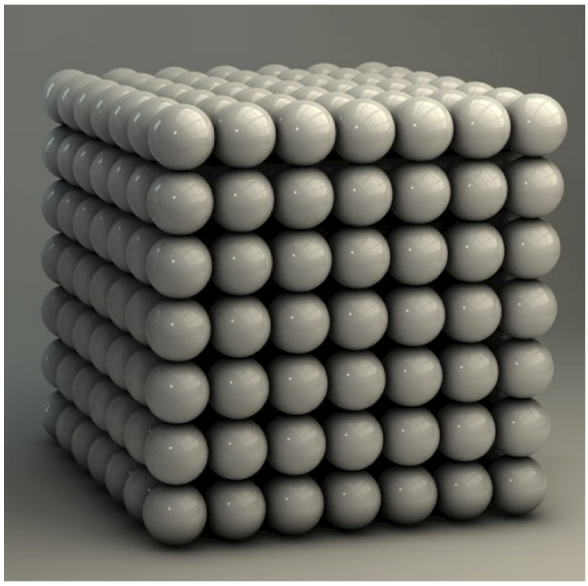

Figure 2.4: Ionic repulsive balls - the assumption Makishima Mackenzie model makes for glass (26)

2.4.2 Borate Glasses

Unfortunately, while equation 2.32 works well for predicting the elastic properties of silicate glass, it appears to fail rather badly for borate glass.

Material	Makishima Mackenzie	Experiment
Silicate Glass	79.6 GPa	73 GPa
Borate Glass	114.4 GPa	17.4 GPa
Phosphate Glass	36.8 GPa	31.3 GPa
Germanium Glass	66.7 GPa	43.3 GPa

Table 2.1: Makishima Mackenzie Young's modulus predictions vs experimental values

Makishima Mackenzie Young's modulus predictions vs experimental values. (27)

To explain this discrepancy, the original paper proposes that the value of dissociation energy calculated from the B_2O_3 crystal is too high: "The low Young's modulus of boric oxide is probably caused by the weak binding forces between planes of interlinking BO_3 triangles." The paper compares this structure to the structure of graphite, with strong intra-planar bonding, but weak inter-planar bonding. To calculate the strength of these proposed inter-planar bonds, the authors inserted the experimental value of the Young's modulus for borate glass and the packing density into equation 2.32 ($E = 2GV_t$), and solved for the dissociation energy. They then took this value of G and defined it to be the dissociation energy of bonds on four coordinate boron centres in the glass, called G_4. G_4 was more than four times smaller than the experimental value of G for B_2O_3, which they defined as G_3. They proposed that G_4 would apply to all BO_4 cross linking centres in the glass, while G_3 would apply to BO_3 centres. They then substituted G in equation 2.32 with

$$G_B = \gamma(G_4 - G_3) + G_3, \tag{2.36}$$

where $G_4 = 15.6kJ/cm^3$ and $G_3 = 111.5kJ/cm^3$. They used estimations of what the ratio γ would be for unknown glasses, not proposing a method for determining this ratio. With this new adapted value for the dissociation energy, with input variables defined by experimentally derived output values, they were able to get more reasonable predictions for the Young's modulus of B_2O_3 glass.

There is little theoretical or experimental basis to believe this assumption about two different types of bonds in borate glass is correct. Recent DFT and MD calculations performed by Huang et al. (12; 13) propose a variety of possible B_2O_3 structures, including an amorphous (glass-like) phase, that match experimental properties. None of these structures has a layered graphite style structure, and all the bonds are of equal and high strength. The assumption made in the MM model for borate glass appears to be unjustified. More troublingly, the method of determining the G_4 constant is by working backwards from the experimental elastic properties of borate glass, turning the model on its head. The G_4 constant is essentially an empirical fix to the poor theoretical prediction, with flimsy reasoning to back it up. This suggests that something is breaking down with the model, when such a fix is required for such a broad set of glasses.

Chapter 3

Method

A set of programs and scripts were created to test different aspects of the Makishima Mackenzie model. There where two core programs used: LAMMPS (28), and a custom code for generating LAMMPS input and managing its output. LAMMPS is a large classical molecular modelling program with a wide array of functions and applications, and it provides the core energy minimization and elastic potential calculation capability that generated the results in this thesis. It was chosen for its free and open source nature, power, and customizability. The custom input generator and output manager code allows for the tuning of input experimental systems for LAMMPS and analyzing the output for different metrics. The scripts used were to run multiple calculations at once, to vary deletion parameters, calculate various properties, and generate streamlined output for data analysis.

3.1 LAMMPS Calculations

The calculations of the elastic constants were performed in LAMMPS. The key method used by LAMMPS to determine the elastic constants was outlined in the previous theory chapter. This equation for elastic constants in terms of the change in the pressure tensor and the change in strain was used in equation 2.19:

$$\frac{\partial \varepsilon_i}{\partial \sigma_j} = c_{ij}.$$

The general structure of the calculations can be found in the elastic example provided with LAMMPS. The first step in performing the calculation involved inputting the details of the structure being modelled, structures that were generated by the custom input code. Specifically, the atomic positions, bonds, atomics, and unit cells vectors were input and defined to be fully periodic. Next, the potential was defined, and so were the parameters for minimization, in particular the convergence criteria. The conjugate gradient minimization method was used for these calculations, with convergence occurring once forces fell below 10^{-10} eV/angstrom. Then the energy of the system was minimized, and the unperturbed pressure tensor elements calculated.

Twelve different strains were applied to the system, one positive and one negative strain in each of the six independent directions, as defined by the strain and stress tensors. The change in each of the six pressure tensor elements was calculated for each of these strains. For the symmetric positive and negative strains, the change in each pressure tensor element is theoretically equal for small strains, so the average of the two changes for the same pressure tensor element was taken:

$$\left(\frac{\partial \varepsilon_i}{\partial \sigma_j(+)} + \frac{\partial \varepsilon_i}{\partial \sigma_j(-)}\right) \Big/ 2 = c_{ij}. \tag{3.1}$$

The two separate strains are applied only in the positive or negative direction and averaged together. From the combination of each of the six strains and six pressure elements, the 36 elastic tensor elements could be calculated.

3.2 The Potential

The potential used for the energy minimizations and pressure tensor calculations was a combination of a harmonic linear bond potential and a harmonic angle potential. The bottoms of the potential wells, or the zero potential energy points, were set at the average bond length and bond angle of Si-Si bonds in diamond cubic pure silicon.

The k constant values for the two angle and bond potentials were determined by calculating the series expansions of the Stillinger-Weber (29) potential at the same minimum energy diamond silicon angle and bond lengths, and using the constant in front of the quadratic term for k. There are two additive parts of the Stillinger-Webber potential, a linear bond energy and an angular bond energy, hence the use of both a linear and angular harmonic potential, and therefore two different k values.

The Stillinger-Weber potential was chosen as it does a good job of predicting experimental elastic constants for pure silicon, and so to see in further experiments a good approximation of the effect on experimental elastic constants from different manipulations of the input structure. The reason the potential was simplified to a set of harmonic potentials was that it would reduce the computational load, that since only minor perturbations would be applied the reaction of the potential energy would be very similar, and most importantly that it allowed the break down of the potential and specific bonds so the bonding structure could be investigated in a number of different ways. The elastic properties generated from the harmonic potentials matched those for the full potential for fully bonded Silicon.

3.3 Input Generation

A program was written to be able to control the atomic and bonding structures input into LAMMPS. In the program, there are two core classes that define the functioning of this program: the atom class and the function class. The atom class contains all functions for manipulating atoms and for calculating their various properties and relationships. It also stores all atom data, primarily the atomic positions, the list of atoms, and the adjacency matrix for all atoms. Where the atom class stores the actual data about the atoms, the function class contains the data about the bonding of the atoms, allowing for the bonding system to be manipulated without losing information about the atoms and their nearest neighbours. In figure 3.1, this separation between

the two classes is shown.

The input for the generator is any unit cell with an orthogonal set of cell vectors, and a set of starting atom positions in equilibrium. It then increases the size of the cell to that desired by the user. For all the calculations performed here, a 4096 atom cell was used as at this point the elastic properties were found to be converged for partially bonded systems. This cell increase is done by simply duplicating the contents of the cell along each cell vector any number of times. Next, based on a user input distance of nearest neighbours in the input cell, the nearest neighbour list is created for the enlarged cell.

Once the bonding system is prepared, a series of different methods are available for changing the bonding structure of the cell, and these will be further elaborated in the following sections. However, all these methods have a key deletion algorithm in common. This algorithm randomly removes bonds from the system based on a specific constraint: that no atom may have fewer than two bonds. That constraint is chosen because an atom with fewer than two bonds is effectively removed from the system; bonding effects are the only forces an atom exerts on the system and a single hanging bond will always sit at zero energy. It is undesirable to have atoms effectively removed from the system in an algorithm for deleting bonds.

The algorithm is constructed so as to maximize efficiency of the run, as these methods run in large nested loops, resulting in a large number of bonds. The way the algorithm does this is by making a random selection and removing ineligible bonds from the list at the same time. First, a list of eligible bonds for deletion is generated. The challenge is that this list of eligible bonds is no longer totally correct once bonds start being deleted, since some bonds that were once eligible for deletion without breaking the constraint had too many neighbours removed and thus they are no longer eligible. Therefore, the algorithm must randomly choose a bond from a list of unknown length, removing ineligible bonds from the list as it encounters them, and

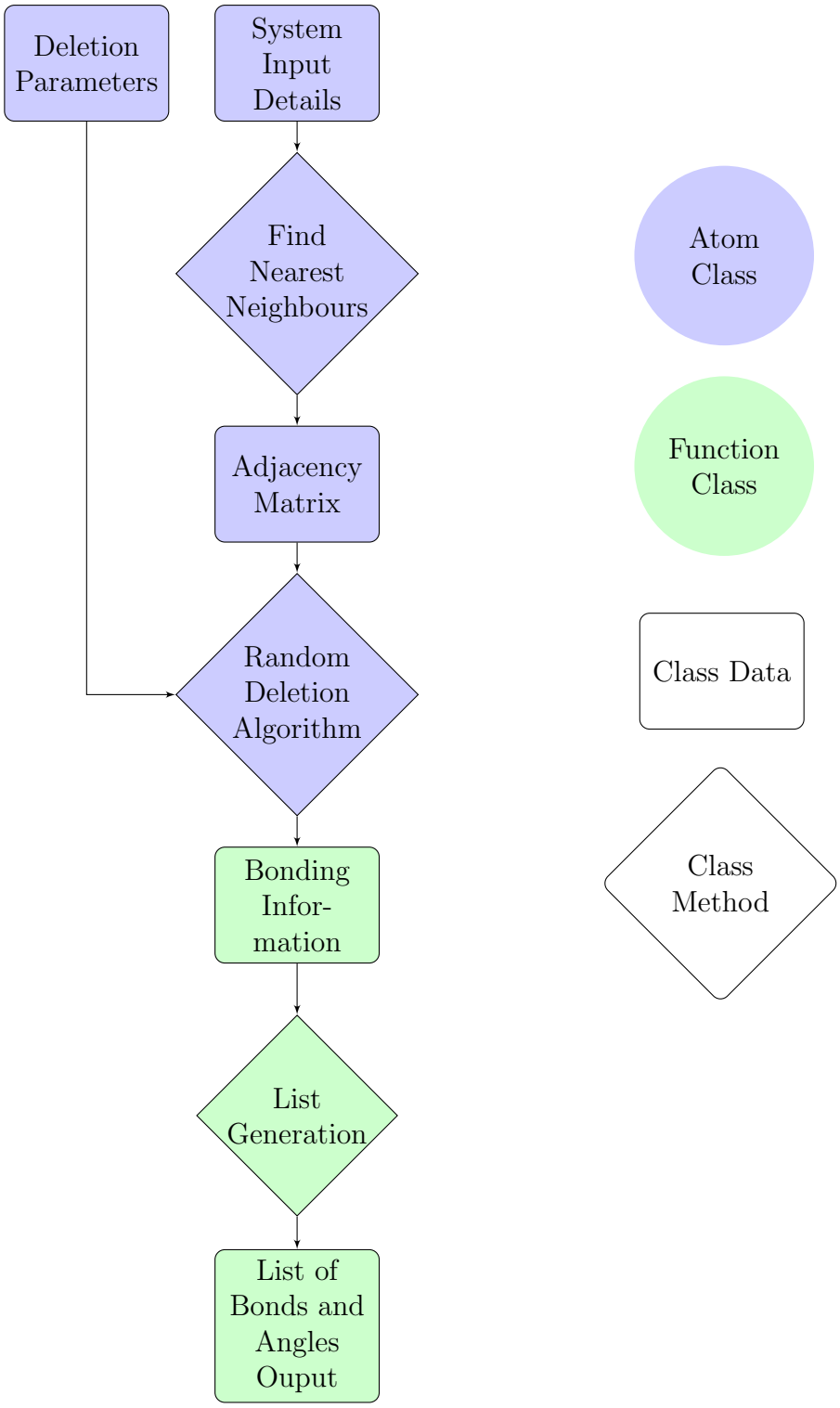

Figure 3.1: The structure of the random deletion input generation program

it ideally does this in a single loop. The solution is to hold the first eligible candidate in memory, and have a random chance of replacing it with another eligible candidate further down the list, with the probability this replacement decreasing the farther into the list the algorithm progresses. When the end of the list is found, the candidate left in memory has been randomly chosen from the list of eligible bonds for deletion. The result is a random selection.

This algorithm is looped to perform as many random bond deletions as desired to get the desired level of bonding order in the structure. Additionally, by modifying the restrictions, the structure can be tuned to have different bonding orders. These 'guided' deletions are described in the next section. Additionally, atoms can be randomly deleted just like bonds, with the same algorithm used. The restriction on the atomic deletion algorithm is that atoms cannot be deleted that would reduce their neighbours below two bonds. This is again chosen so that only the specified atom is removed from the system, and other atoms are not accidentally deleted while the program still thinks they are within the bonding structure.

Once the list of bonded atoms is finalized, a full bonding list and an angle list are generated for output to LAMMPS. These two lists correspond to the two potentials outlined in the potential section. New cell vectors, the atom list, bond list, and angle list are output to an input file for LAMMPS. Additionally, a number of metrics about the system are prepared: average coordination number, density, bond density, the number atoms of each coordination, the average coordination around each specific coordinate atom (i.e. the average coordination of the neighbours of 4, 3 and 2 coordinate atoms), and a few other parameters that provide information about the run of the program. From this point, a LAMMPS run can be undertaken to calculate the elastic properties of the generated system.

Additionally, a small output manager protocol was added to the same input generator code. This protocol has the simple function of taking LAMMPS output atomic

positions and bonding connections and returning a list of atomic or bonding positions in a different format.

3.4 Methods for Guiding Deletion

The core function that determines the conditions for deletion eligibility has a number of different options available to change the way bonds are deleted. That way, instead of random bond deletion, there are now have semi-random forms of deletion that can affect the resulting structure in various ways. The core mechanism for determining candidates for deletion is based on setting the minimum bond order on the atoms on either side of a bond. For the random deletion, these minima are set at two for both atoms in the bond. The first form of guiding is to restrict the minima to be 3 and 2. The purpose of this is to approximate a structure similar in bond order to B_2O_3. Another guiding method involves restricting the deletions to only coordinations of 3 or greater on both atoms. These types of restrictions greatly limit the number of bonds that can be removed from the system.

The next methods of guiding deletion involve setting triggers at which point the conditions for deletion change. This allows the removal of bonds from a highly restricted set, then allows further deletions from a less restricted set. The first of these methods only allow a minimum of 3 coordination on both atoms at first, and then allow deletions down to coordinations of 2. The point at which the restriction change is triggered can also be modified. The trigger is a comparison of the number of 4 coordinate and the number of 3 coordinate atoms in the structure. The trigger is set

to occur in three different ways:

$$5 \times \#\text{ coord } 4 = \#\text{ coord } 3$$

$$\#\text{ coord } 4 = \#\text{ coord } 3$$

$$\#\text{ coord } 4 = 5 \times \#\text{ coord } 3$$

This way highly restricted deletions can be occurring for only a short time, or the restrictions can be reduced once almost all eligible bonds are removed. The last deletion guide based on bond order restrictions used was to restrict deletions to 3 and 3 coordinate bonds, then allow 3 and 2 coordinate bonds. Figure 3.1 summarizes these different methods. The first row defines the number of the deletion (0 for random deletions). The second row defines the minimum coordinations on bonded atoms at the beginning of the deletion cycle. The third row defines the comparison between counts of each coordination that triggers the change to different minimum bonded coordinations. For the deletion guides that do not change, numbers 0 through 2, no trigger is specified. Finally, the last row defines the new set of restrictions on bonded coordinations.

#	Initial Restriction	Trigger	Final Restriction
0	2, 2		2, 2
1	3, 2		3, 2
2	3, 3		3, 3
3	3, 3	$5 \times \# 4 = \# 3$	2, 2
4	3, 3	$\# 4 = \# 3$	2, 2
5	3, 3	$\# 4 = 5 \times \# 3$	2, 2
6	3, 3	$5 \times \# 4 = \# 3$	3, 2

Table 3.1: The different deletion guides

The final method of guiding deletion was to introduce a bonding phase difference within the cell. This is accomplished by the restriction of all deletions to within a certain radius from the middle of the cell. The result of this restriction is that the

outside edges of the cell have fully coordinated bonds, while the interior of the cell has a highly decimated structure. The result of these different deletion guides is that the effects on elastic properties from different coordination distributions can be examined.

Several metrics are determined about the input generated. The state of disorder in different distributions can be estimated through the equation

$$\sigma = \sum_{n=2}^{4} x \cdot ln(x), \text{ where } x = \frac{\#n \text{ coord}}{\#\text{ atoms}}. \tag{3.2}$$

Also measured is the average coordination number of atoms bonded to each specific coordination. For instance, the average coordination of atoms bonded to 3 coordinate atoms. This provides information on how close different deletion guides get to similar experimental systems.

3.5 Measurement of Voronoi Cell Volumes

One additional measurement made of the structures generated was to calculate their average Voronoi cell volumes and the distributions of those volumes. Voronoi cells are defined for any system of points in space. In these measurements, the system of points are either atoms positions or bond midpoints. A Voronoi cell around an atom is defined as the set of points closer to that atom than any other atom. An illustration of Voronoi cells is shown in figure 3.2.

In other words, the Voronoi cell defines the space nearest to an atom. This measurement can be of use as it allows the measurement of the amount of empty space in the cell. As the Voronoi cell size grows, the distances between the atoms or bonds grow and there is more open room inside the cell. The reason for calculating Voronoi cell volumes for both atoms and bonds is that some of the experiments conducted in this work involve the deletion of bonds while keeping atoms constant, and others remove atoms. Voronoi cell volumes only centred on atoms would be constant for the

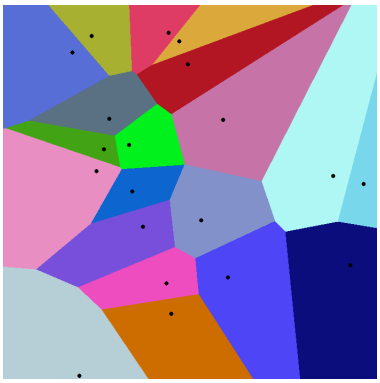

Figure 3.2: A 2-D example of Voronoi cells (30)

bond deletion experiments. The output manager described in the Input Generator section was used to take LAMMPS output and process it into either atomic or bond positions for Voronoi cell calculations. The Voronoi cells themselves were calculated with voro++. (31)

3.6 Submission Scripts

A few different scripts were written to streamline the running of these different programs together and to vary the input variables. The basic submission script performs increasingly large deletions as a percentage of the overall number of bonds in the system. Each deletion is run 20 times and the average taken to smooth out the random variations in each individual run. To accelerate this process, and as the custom program is not multithreaded, each individual run was submitted to one computational core, allowing the performance gains of multithreaded calculation without major software engineering investment. Finally the script parsed the LAMMPS results for the key output parameters and generated output for data processing in Excel.

From this basic input script, a number of modifications were written to calculate various properties, including the ones described in previous sections of this chapter. There were scripts written for each of the guided deletion methods. A script was created for the radial deletion guiding that looped over different values of deletion

radius. For the Voronoi cell calculations, a script was made that took the output from the LAMMPS calculations, processed it with the output manager, and ran voro++ (31) on it. Additionally, there was a script that ran different combinations of atomic and bond deletions to see what effect these different deletions had on the elastic properties. And finally, a script was made that varied the Stillinger Webber derived k constants for the angle and bond harmonic potentials, to see which of these potentials had a greater effect on elasticity.

Chapter 4

Results

The first set of results and the largest quantity of them was from the different randomized bond decimations. In the following graphs (figures 4.1 through 4.9), two key sets of data about the calculated systems are reported: three elastic constants, c_{11}, c_{12}, and c_{44} (the 3 sets of stars); and the absolute number of atoms with the 3 possible coordination numbers of four, three and two (the 3 coloured lines). This data was collected to test the relationship between the average coordination number and elastic properties. Additionally, data is plotted on atom decimation, to see the dependence of elasticity on density. Next, data on the level of bonding disorder in the system is presented in figure 4.10 for the different deletion guides, to determine the dependence of elastic properties on the bonding distribution in the system. Following that are a series of graphs on Voronoi cell calculations for the random deletion calculation: figures 4.11 through 4.15. These graphs attempt to see what relationship there is between void space in the system and elastic properties. Finally, figures 4.16 and 4.17 present data from modifying k values in the potential, to see how different potential strengths affect the elasticity.

4.1 Random and Guided Deletion

In the figures on random and guided deletion, the coordination counts and elastic constants are plotted in terms of the average coordination number of the system, which at the left of the graphs is 4 for a fully coordinated diamond lattice, down towards an average coordination number of 2 for the systems which were the most

decimated. The left most data point is the same on all the following graphs, and the different coordination distributions show how the different deletion guides operate. The elastic constants are all reported in gigapascals on the right y axes, as is standard for elastic properties. The coordination counts are reported on the left y axes - these correspond to the solid lines, and these, as the average coordination number, are unit-less.

Figure 4.1 shows the results of the random bond deletion experiment. In the fully coordinated system, with 512 four coordinate atoms, the elastic properties match those for the Stillinger-Webber potential: $c_{11} = 151GPa$, $c_{12} = 76GPa$, $c_{44} = 56GPa$ (29). As the random deletion algorithm progresses, a rise and fall in the number of 3 coordinate atoms in the system can be seen, with mostly 2 coordinate atoms present at the end of the run. It's worth noting that the weighted average of the three coordination counts (for 4, 3, 2 coordinate atoms) gives the average coordination number on the x axis. Most significantly, as the average coordination approaches 2.4, the elastic constants all converge to zero and stay at zero for lower average coordinations. This confirms the results of Thorpe (19), and also corresponds to the average coordination number of B_2O_3.

Graphs 4.2 and 4.3 show the results from tightening the restrictions on eligible bond deletions, first to bonds with coordinations greater than 3 and 2 on the bonded atoms, and then with coordinations of greater than 3 and 3. (These guides are the same as those previously outlined in Table 3.1.) This has the effect of limiting the total number of deletions allowed to take place, and thus the calculations terminate at higher average coordination numbers than the random deletion experiment. This is demonstrated in the second guiding, where only deletions from 4 coordinate atoms are allowed, and thus the number of 2 coordinate atoms stays at zero throughout the run. There are fewer snapshots taken in the experiments after the random deletion experiment, as the same overall trends can still be seen, which is why fewer points for

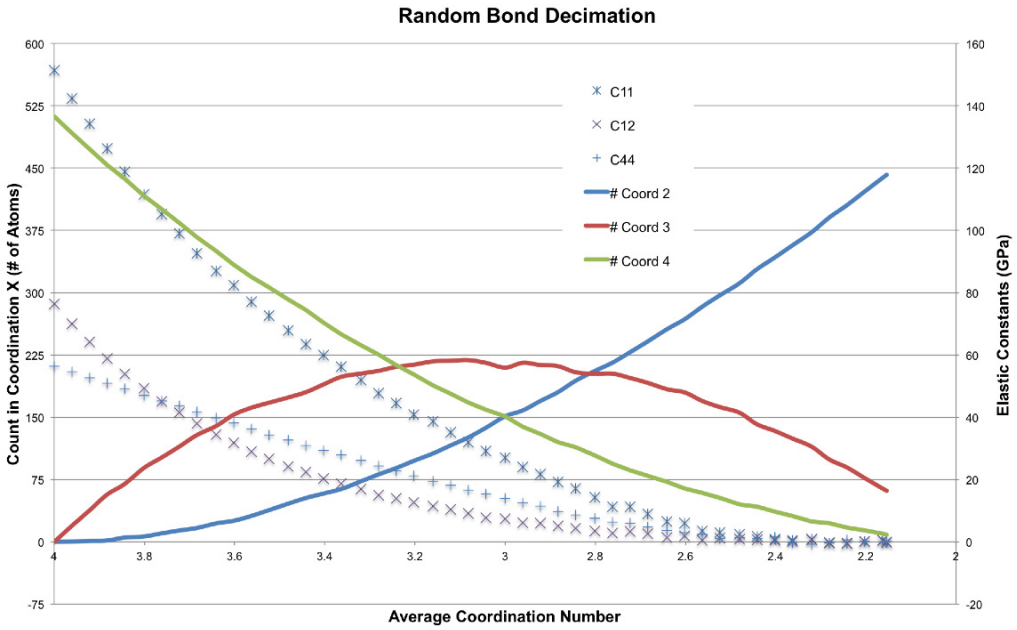

Figure 4.1: Random bond deletion in a diamond lattice

the elastic constants appear. The problem with these deletion guides two and three is that the high restrictions prevent the average coordination number from decreasing down to the area relevant to B_2O_3. That is why the next deletion guides changed the restrictions at some point during the calculation, to allow access to lower average coordination numbers.

In the next set of guides (figures 4.4 to 4.6,) the high restriction of no coordinations below 3 is chosen at the beginning of the run, and then relaxed to allow coordinations of 2 at various points in the run. This results in different distributions of coordinations throughout the runs, while still allowing the system to reduce to low average coordination numbers. Despite the significant differences in the coordination distributions, the elastic constant curves still follow broadly similar shapes to the random deletion experiment, and go to zero around an average coordination of 2.4. This demonstrates that the key factor in determining overall elastic properties is the average coordination, while varying the distribution of those coordinations only has subtle effects on the properties. (The plot for guide 6 is not presented, as it is not

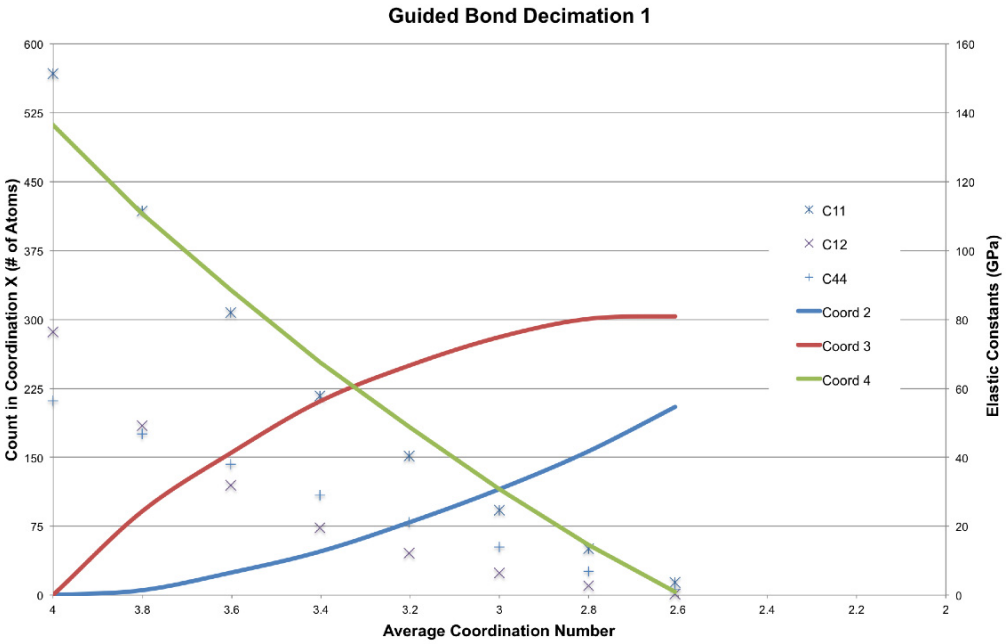

Figure 4.2: Guided semi-random bond deletion #1

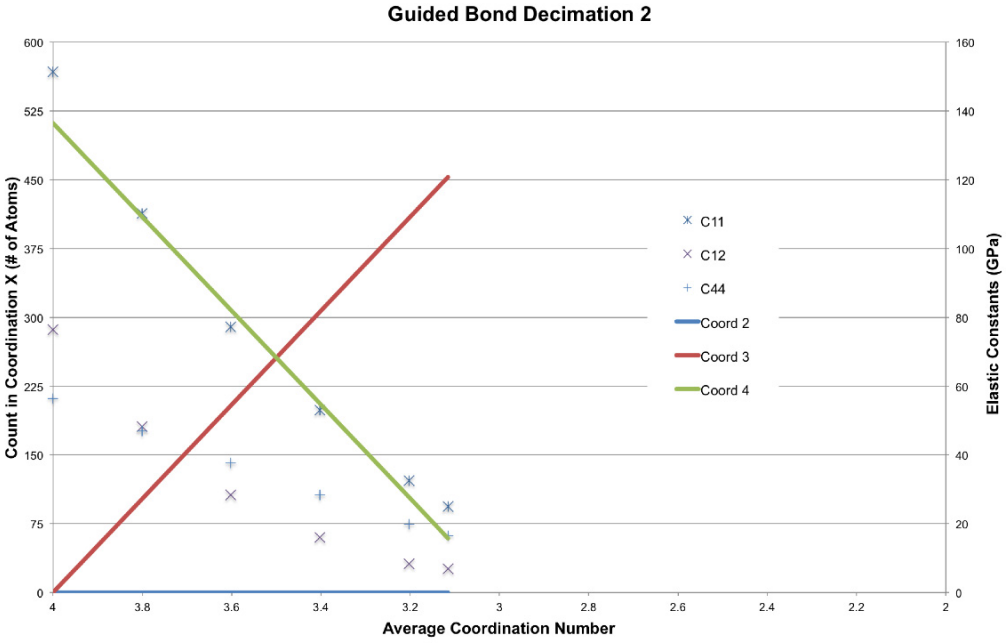

Figure 4.3: Guided semi-random bond deletion #2

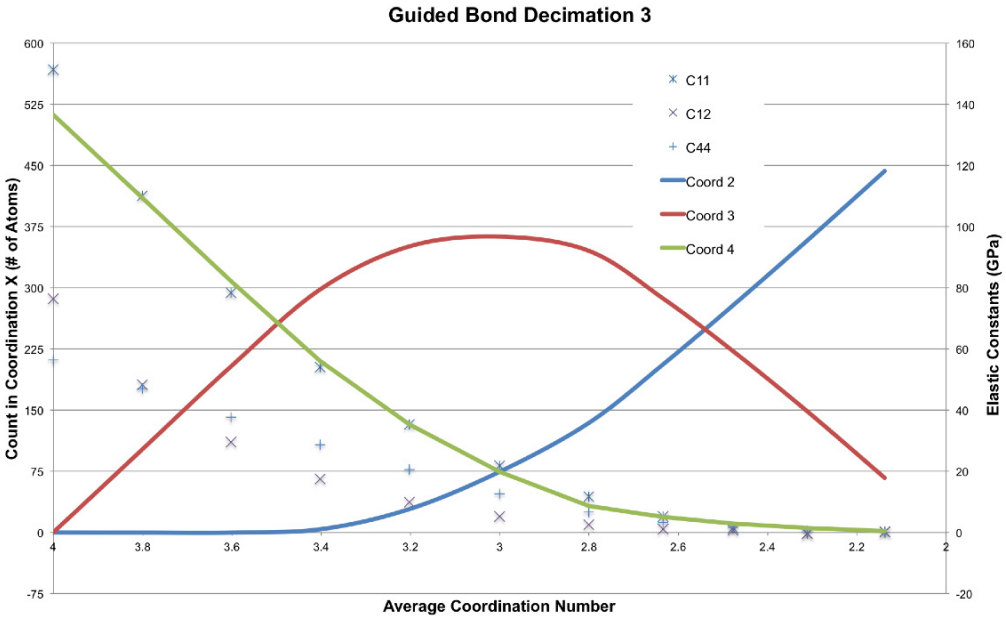

Figure 4.4: Guided semi-random bond deletion #3

meaningfully different from the plot for guide 2, since the ending restriction is the same.)

For last guide on bond deletions (figure 4.7,) an increasingly large radius of possible deletions was chosen, and the elastic properties calculated. At the maximum deletion radius, the experiment is equivalent to a perfectly random deletion. At small deletion radii, there are essentially have two phases in the solid, one of highly decimated bonding near the centre of the cell, and another of full coordination around the outside of the cell. Plotted in figure 4.7 are all of these experiments against their average coordination numbers. These phase differences do indeed appear to have an effect on the elastic properties at higher coordinations, as demonstrated by the spread in the data. However, at coordinations of 2.4 and lower, all elastic properties fall to zero, even for experiments with a radial deletion restriction.

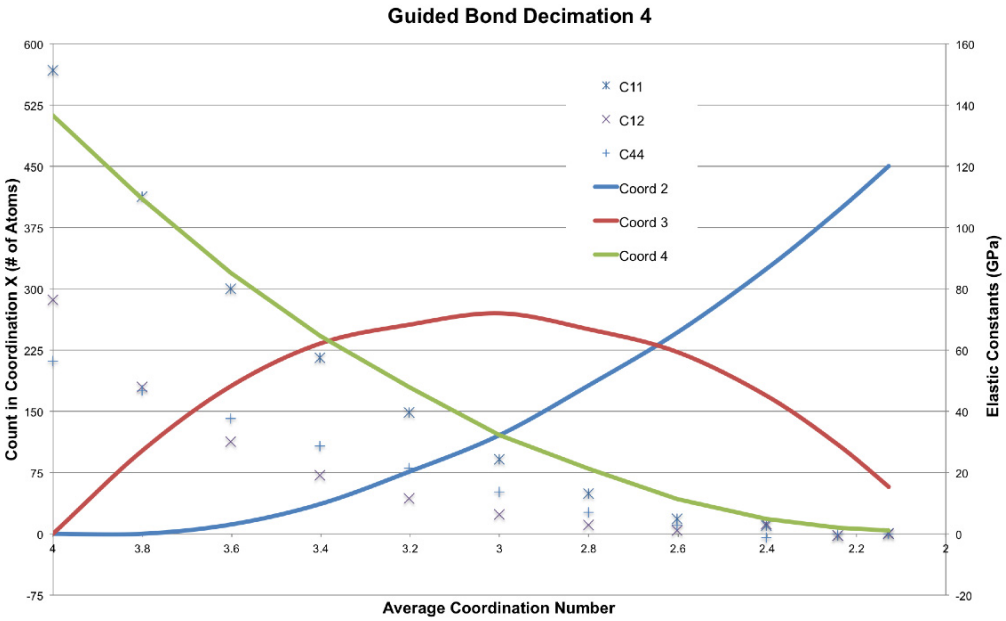

Figure 4.5: Guided semi-random bond deletion #4

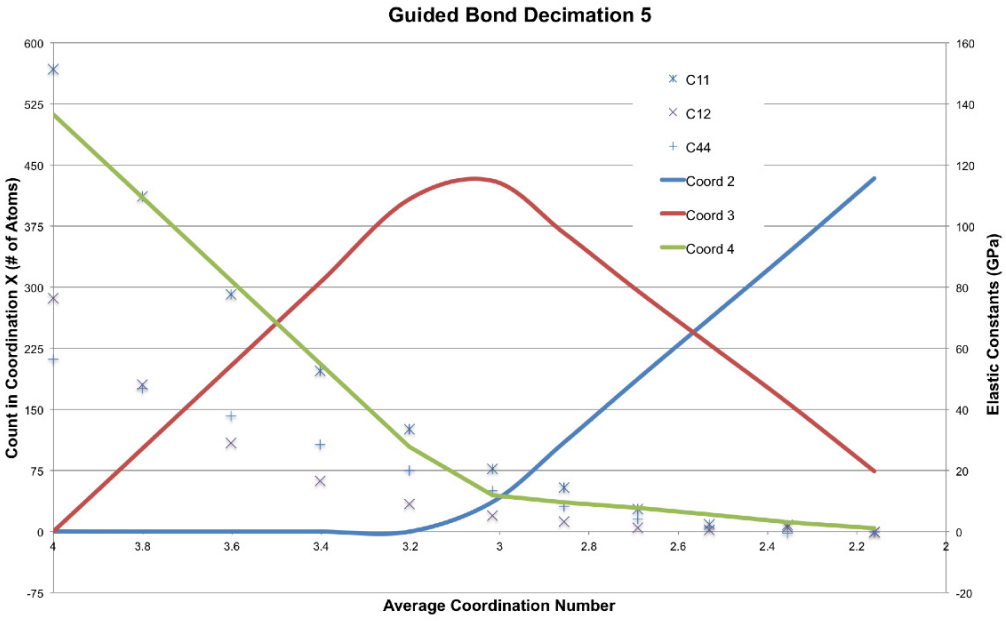

Figure 4.6: Guided semi-random bond deletion #5

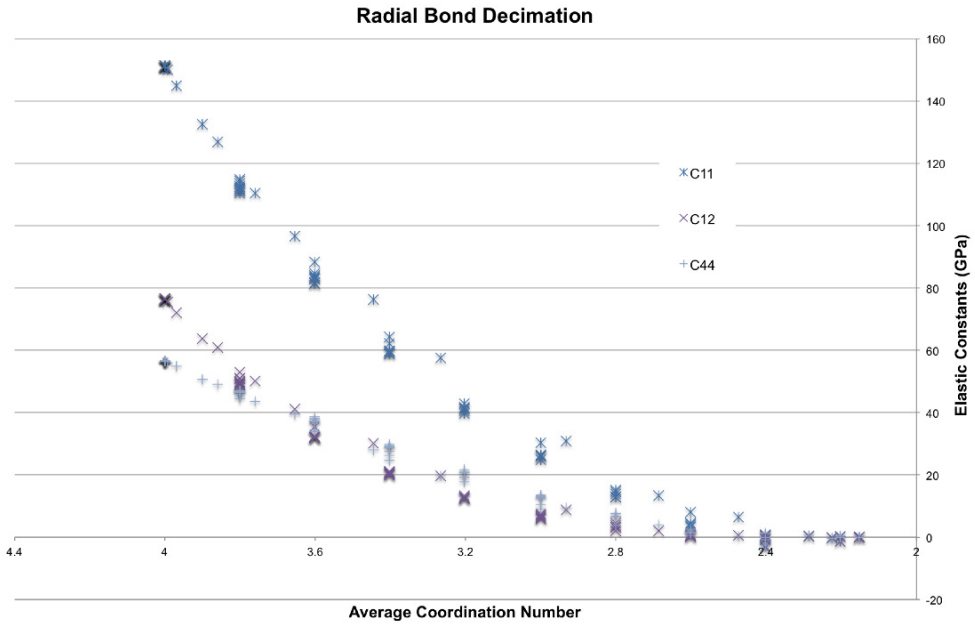

Figure 4.7: Radially guided semi-random bond deletion

4.2 Atom vs Bond Deletion

For the next two figures(4.8 and 4.9,) some of the deletions are atom deletions rather than bond deletions. Here atoms are removed (and all bonds attached to them) rather than bonds being removed. In the first of these graphs, only atoms are being removed and bonds are not independently removed. The results match those from the random bond deletions, trending to zeroed elastic constants at an average coordination of 2.4. It is important to emphasize, in this experiment, because atoms are being deleted from a cell of fixed size, the density is being reduced. In previous experiments, the density throughout the deletions remained constant, as no atoms were removed. Thus it is the average coordination number that has the bigger effect on the elastic properties, not the density. Indeed, in figure 4.9, the bond and atom deletion experiments are mixed. Every combination of atomic and bond deletions is plotted, from no deletions, through 5% atom and 45% bond deletions, to 45% atom and 5% bond deletions. The result of this is that there is a broad range of different atom densities appearing as

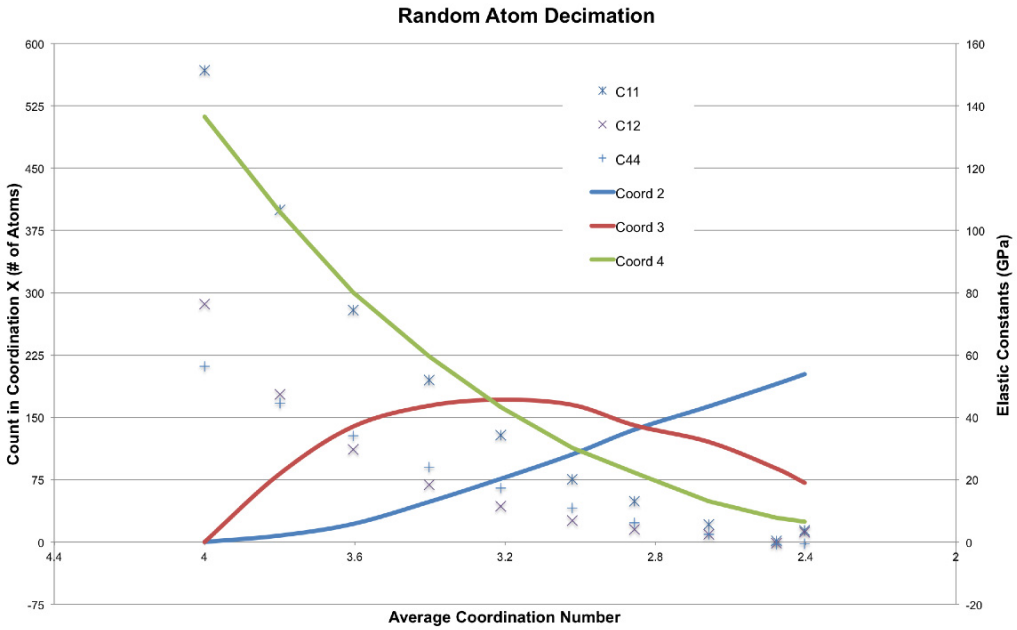

Figure 4.8: Random atom deletion in a diamond lattice

different markers in the plot. All these combinations of deletions fall on the same trend line, and they approach zero at the same key average coordination number of 2.4. The elastic properties appear to be independent of density for this system.

4.3 Effect of Disorder on Elastic Properties

Since there were so many different guides developed to change the bonding distributions in the system, the disorder of the bonding distributions was measured, and is plotted in figure 4.10. Equation 3.2 defines the x axis in this plot. It can be seen that there is no direct relationship between the distribution of coordinations in the system and the elastic properties.

4.4 Voronoi Cell Distribution

With the previous results suggesting the importance to the elastic constants of the average coordination number over other properties of the system, measurements were

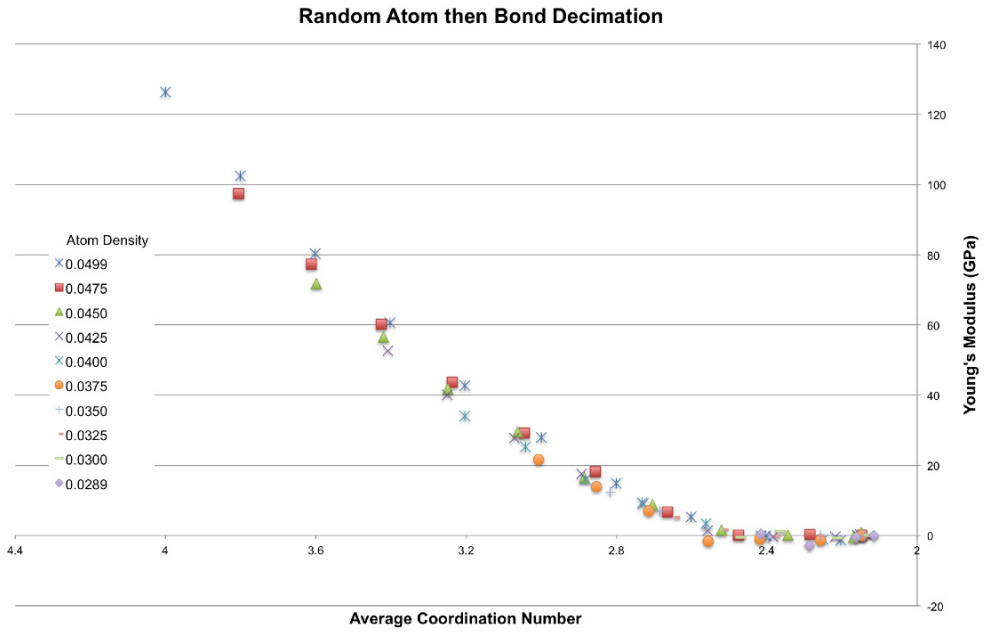

Figure 4.9: Combined random atom and random bond deletion in a diamond lattice

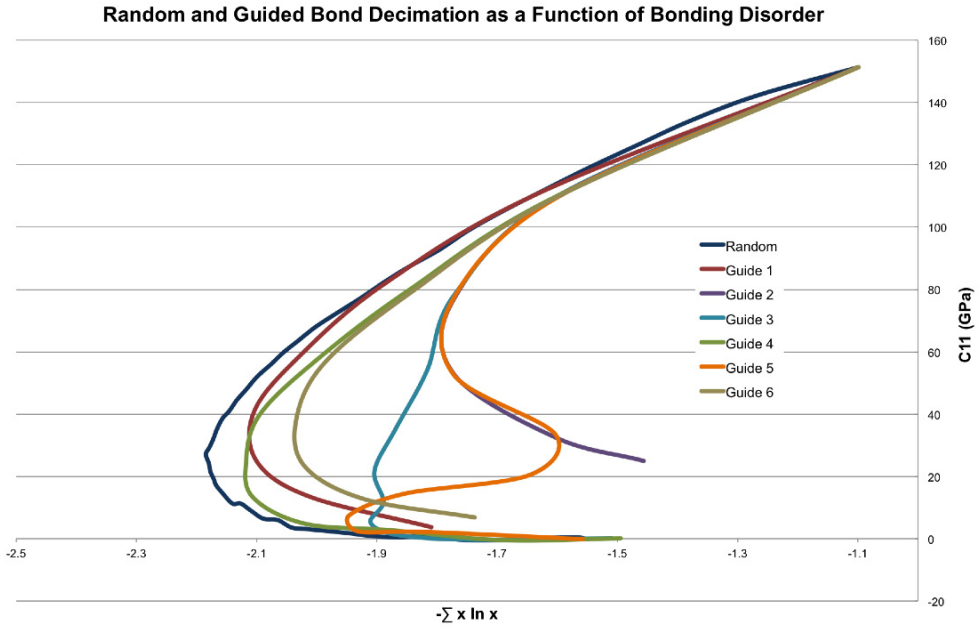

Figure 4.10: C_{11} vs. disorder in coordination distribution

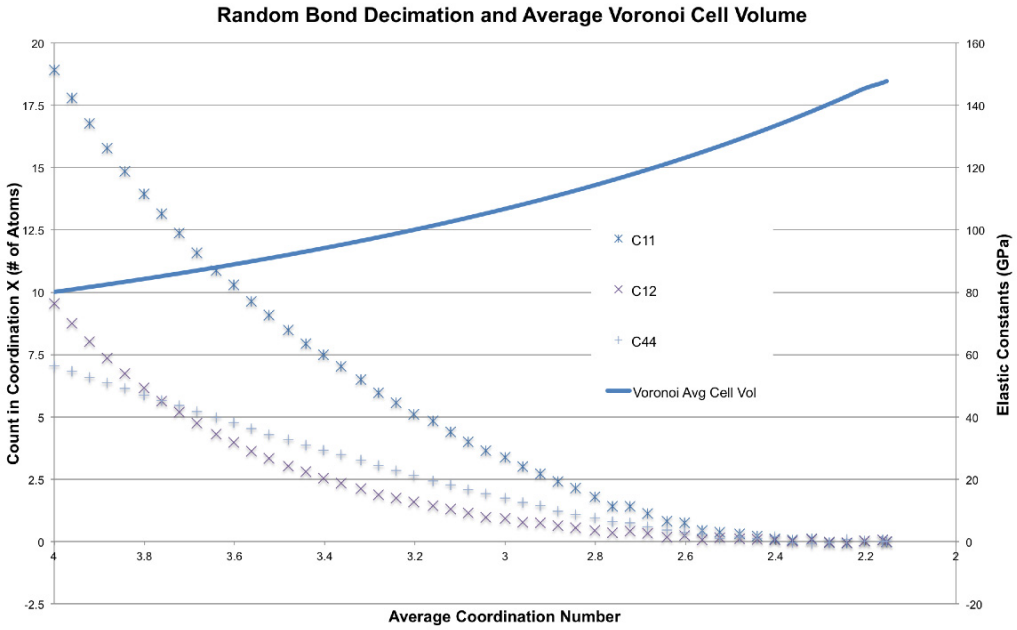

Figure 4.11: Average Voronoi cell volumes

taken with the goal of divulging the key reason behind the importance of the average coordination number. The choice was made to measure the Voronoi cells of the bonds in the random bond deletion experiments, to see how the volume available to each bond was changing. In the first plot, figure 4.11, the average Voronoi cell volumes around each bond are plotted as bonds are removed from the system. These results are unfortunately not very informative, and in retrospect, rather obvious. One would expect the average cell volume to rise around remaining bonds, as bonds are removed from the system. These values could in fact be directly calculated from the total volume of the system and the number of bonds in the system.

Endeavouring to see if any greater insight can be gained from Voronoi cell volumes, the distributions of the cells were plotted at different average coordination numbers, and a few key plots of these distributions are shown in figures 4.12 to 4.15. For reference, at full coordination, all the Voronoi cells have a volume of 10.01. Thus, they fall in the volume range between 10 and 10.5 $Å^3$, and are marked by the midpoint of that pool at 10.25 $Å^3$. (For convenience, the volume ranges are referred to by their

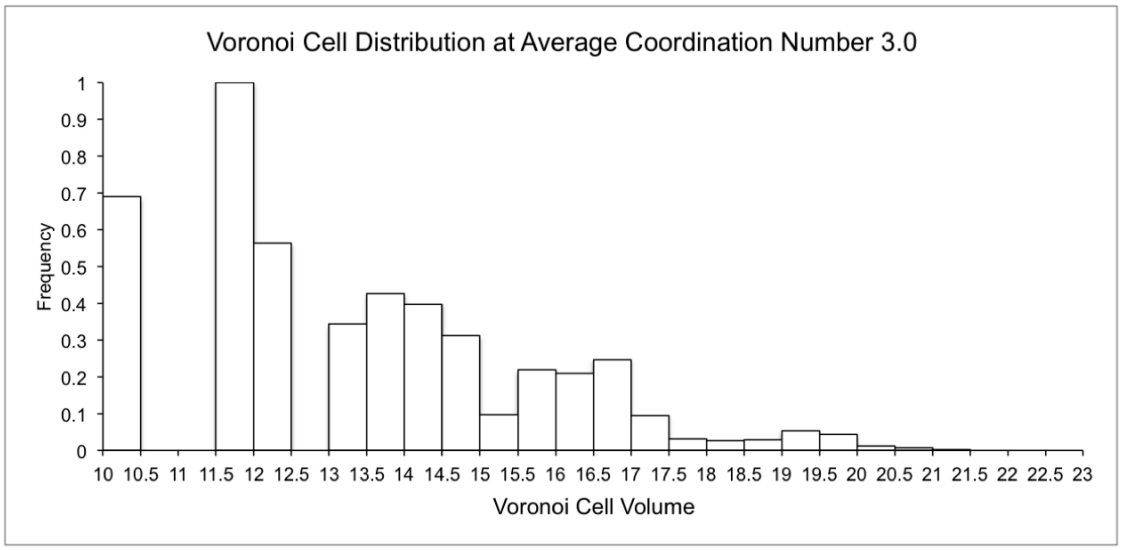

Figure 4.12: Voronoi cell distribution at average coordination 3

midpoint.) It can be seen that even at a much lower coordination of 3, most bonds still have a cell volume not much larger than in the fully coordinated distribution. However, over the progression from a coordination of 3 to a coordination of 2.4, the peak point in the distribution dramatically shifts. The median cell volume increases by 43% from 11.75 to 16.75; in comparison to an increase in the median cell volume of 15% over the larger coordination drop between 4 and 3. This suggests that the number of bonds with large volumes around them has a relationship to the elastic properties.

4.5 Variation of k parameters

One final set of experiments was conducted, to see the dependence of the elastic properties on the k values chosen for the bonding potential (the k values derived from the Stillinger-Webber potential, as defined in the potential section of the Method chapter.) In the final two graphs in this section, figures 4.16 and 4.17, the Voigt average of the Young's modulus is plotted against the k value of either the linear or angular portions of the potential. While one k value is modified, the other k value is kept

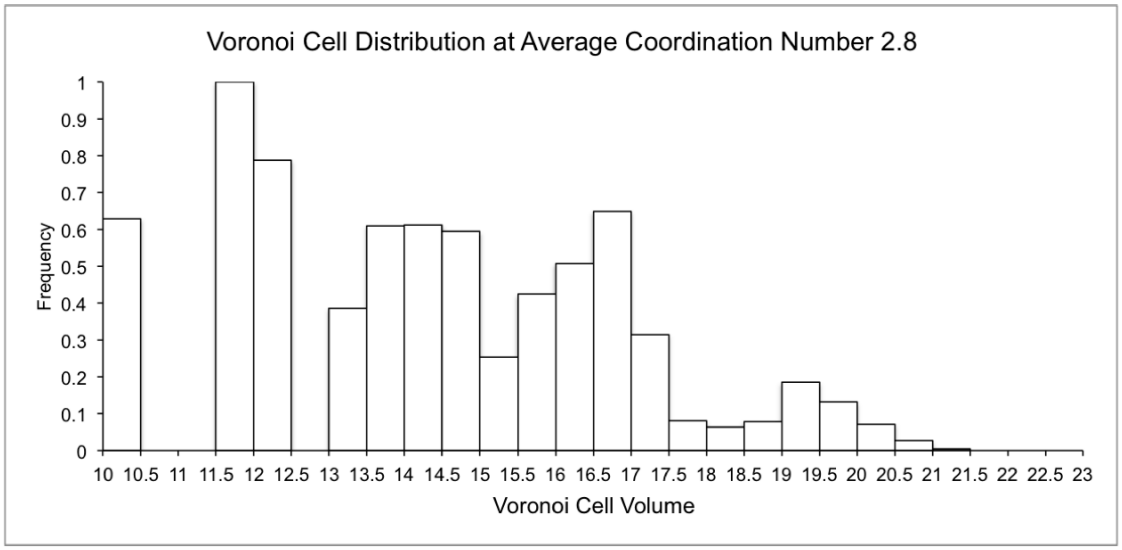

Figure 4.13: Voronoi cell distribution at average coordination 2.8

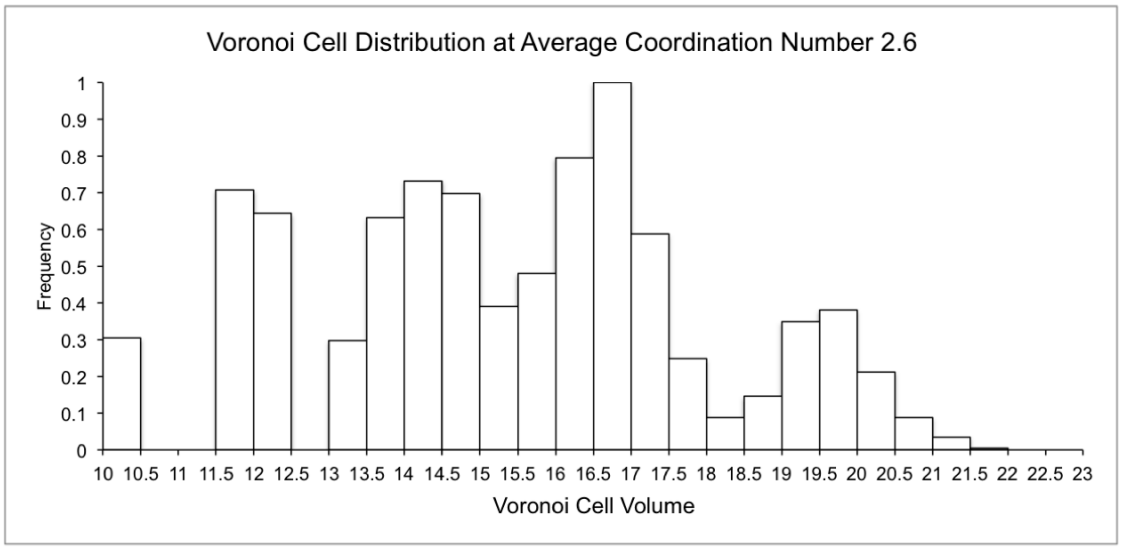

Figure 4.14: Voronoi cell distribution at average coordination 2.6

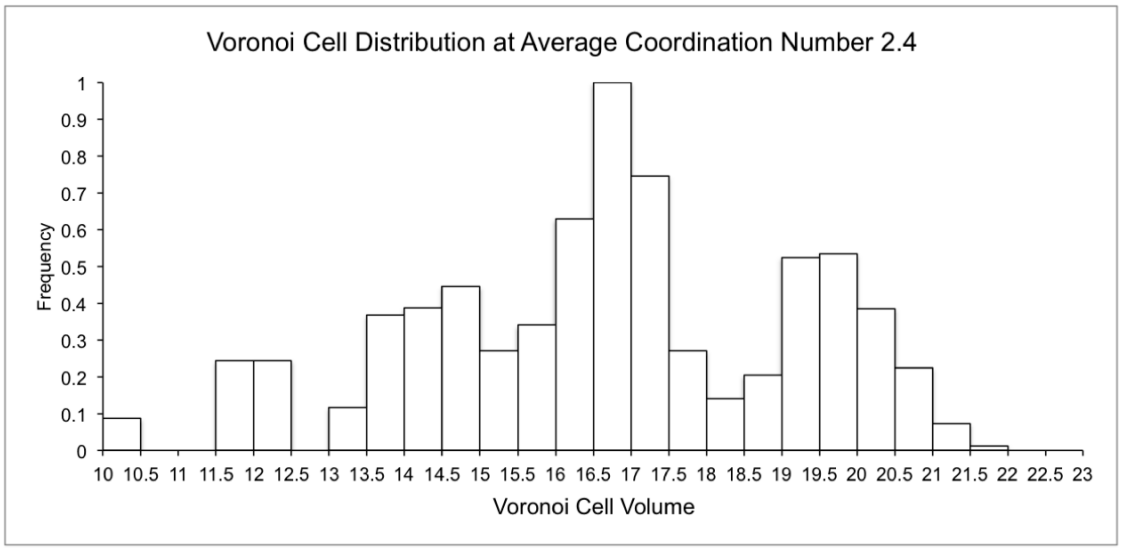

Figure 4.15: Voronoi cell distribution at average coordination 2.4

constant at it default value. The default k's are in the middle of the x axis in both plots at a value of one. The x axis values are normalized to the default value, so the relative scale of both graphs is the same. The dependence of the Young's modulus is plotted with a series of decreasing average coordination numbers, which is why there are multiple sets of data on the graphs.

For the linear k, the plots are roughly flat until the k value approaches close to zero. In contrast, for the angle k there is a linear relationship between the Young's modulus and k value. Indeed, the slopes of the linear trend-lines are four times larger for angular k data sets than for linear k, for all average coordination values. This suggests that forces that restrict the bending of bonds have a larger effect on elastic properties than forces that restrict the compression or stretching of bonds. Notably however, at an average coordination of 2.4, both trend lines had a slope near zero, suggesting no dependency on k values. Of course, at 2.4, the Young's modulus is equal to zero.

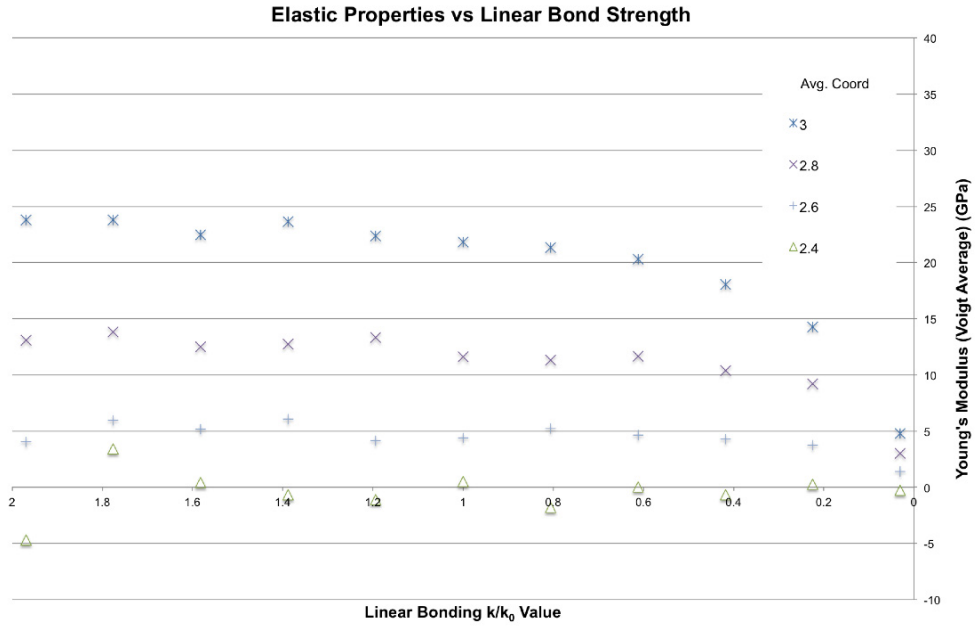

Figure 4.16: Dependence of Young's modulus on the value of linear k

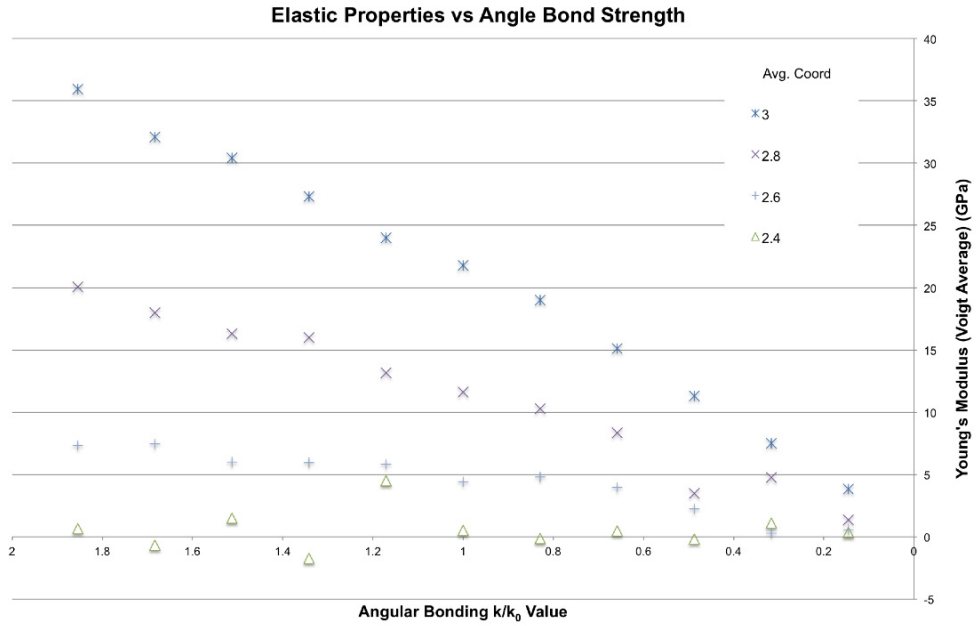

Figure 4.17: Dependence of Young's modulus on the value of angular k

Chapter 5

Discussion

In this chapter, the relationship between elastic properties and various glass properties will be explored: coordination number, coordination distribution, atom density, void space, and bond strength. Two papers by Thorpe will also be examined, and how the structures and theories proposed in them apply to the Makishima Mackenzie model. Finally, all these discussions will be brought together to propose improvements to the Makishima Mackenzie model.

5.1 Importance of average coordination to elastic properties

This section begins by outlining a paper by M. F. Thorpe from 1985, "Rigidity Percolation in Glassy Structures"(19). The theoretical and experimental set-up in the paper is examined, and how it compares to the work in this thesis. The results of that work will also be compared to the results of this thesis. From there, the relationship will be examined between the average coordination number and elastic properties found in these experiments.

5.1.1 Thorpe's Percolation Paper

The paper explores the concept of rigidity percolation, and how it relates to the elastic properties of a basic model system. The paper begins by demonstrating an example of percolation theory: an insulating alloy $RbMn_pMg_{1-p}F_4$, where Mn interacts magnetically with its nearest Mn neighbours. As diamagnetic Mg replaces Mn, the antiferromagnetism of the system falls until the system becomes paramagnetic at

$p \sim 0.31$. At this point there are insufficient nearest neighbour Mn atoms to sustain long range order. Another example is electrical conductivity across a system of wires joined at nodes. The conductivity drops to zero once sufficient nodes or wires have been removed from the system, as there ceases to be a pathway across the system. These examples are part of a class of problems know as connectivity percolation, where overall connectivity is broken across the system, which reduces the measured property to zero.

More interesting is the problem of rigidity percolation. Imagine a 2D triangular net of atoms connected by bonds. When all bonds are present, $p = 1$, the system is rigid, and has defined elastic properties. When all bonds are removed, there are no longer any nearest neighbour interactions and the system is totally fluid at $p = 0$. This breakdown to an unconnected system occurs at $p = 0.35$, another example of the connectivity percolation problem. However, between $p = 0.67$ and $p = 0.35$ the system is geometrically connected (so were it conducting, a current could still flow through it), but the system is no longer elastically rigid and becomes floppy. One can think of a truss bridge structure as an analogy to this. A trussed system of interlinking bars is much stronger than a single spanning bar, much more so than the sum of the bars uses. The network itself imparts very significant strength to the system. Similarly, once enough bonds are removed from network system described in this thesis, the rigidity imparted by the network disappears. There are still rigid pockets in the system, but they are surrounded by floppy regions so the elastic properties of the system become zero. When enough of these rigid pockets are linked, the system regains its overall rigidity. The origin of this concept actually dates back to J.C. Maxwell (32), who asked the question "At what point does a network of bars b and joints j become rigid?"

These ideas were applied to a face-centred cubic system, with a coordination per atom of $r = 4$. The potential used in the system was defined in a previous paper

by Thorpe on the "Effective-medium theory of percolation on central-force elastic networks" (20). The potential simply uses two-body Hookean springs as the bonds, with no other defined forces, just like the model defined in the beginning of the Theory chapter, where the bulk modulus is calculated. The bonds were then randomly deleted from the system, reducing the value of p. They found that the transition from a rigid to floppy system occurred when the average coordination per atom $\langle r \rangle = 2.4$. This is illustrated in figure 5.1, where the elastic constant c_{11} drops to zero at $\langle r \rangle = 2.4$.

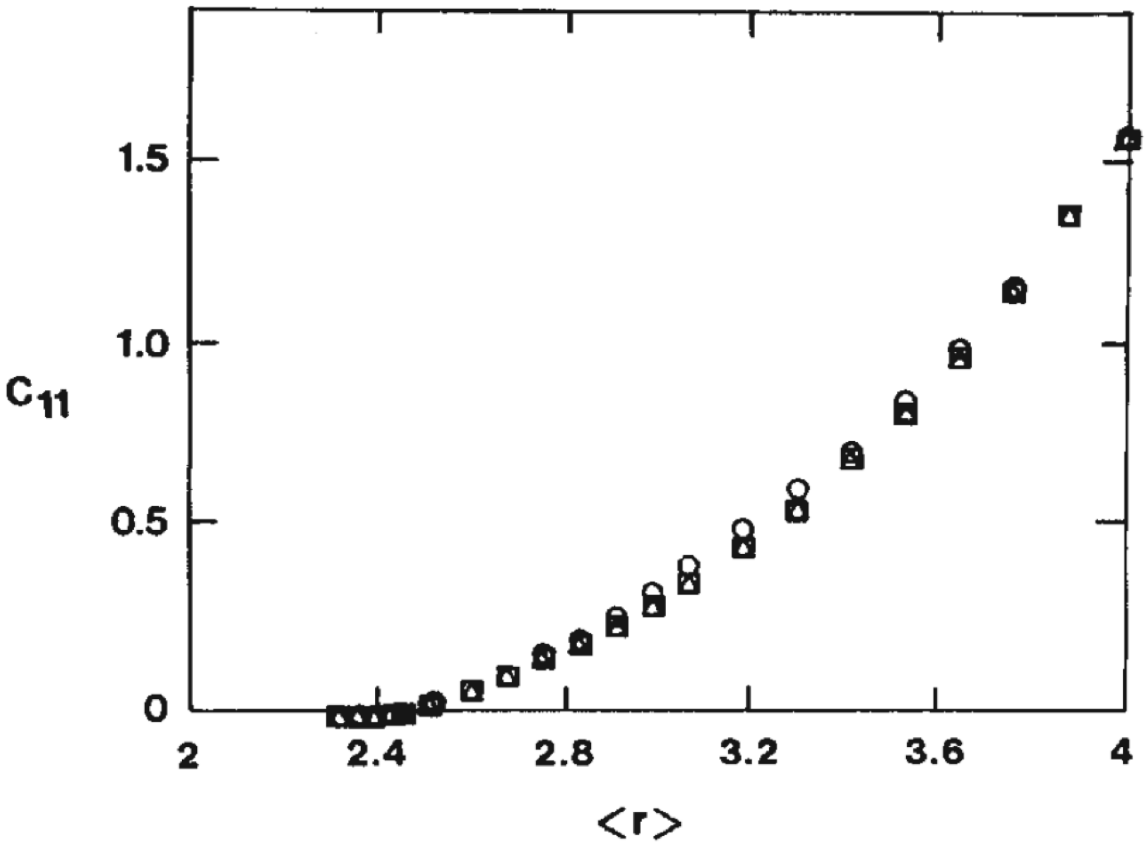

Figure 5.1: The elastic modulus c_{11} as a function of mean coordination $\langle r \rangle$ for three different random networks with 516 atoms each. The different networks are represented by the different point shapes. Figure reproduced from reference (19).

5.1.2 Average coordination in various glasses

Now, in Thorpe's percolation paper, only linear Hookean springs are used for the nearest neighbour forces, and only c_{11} is calculated. In contrast, the potential in this work has included angular Hookean springs, and calculated the full elastic tensor for these systems, as previously described in the Method chapter. As the results repeatedly show, across a wide range of deletion methods from totally random bond deletions, to atom and bond deletions, to locally restricted deletions, and to guided deletions, rigidity percolation in the system ceases at an average coordination of 2.4 every time (figures 4.1 to 4.9). Indeed, all elastic properties fall to zero together at this point, showing rigidity percolation also applies to systems with angular atomic bonding forces. This demonstrates that average coordination is a key element in the overall elastic properties in the system.

This property, coordination, is clearly omitted from the Makishima Mackenzie model in equation 2.32: $E = 2GV_t$. The success of the Makishima Mackenzie model in predicting elastic properties in silicon glasses is due to the coordination numbers present in silicate glass lying in a small range around $\langle r \rangle = 2.67$, as the glass former defines the underlying structure of the system. Borate glasses, in contrast, lie around the threshold of rigidity percolation, suggesting why the Makishima Mackenzie model so radically overestimates the elastic properties.

5.2 Dependence of elastic properties on coordination distribution

To determine the relationship between the coordination distribution and the elastic properties, the five previously outlined guides for deletions were used, plotted in figures 4.2 to 4.6. Only minor variations in the elastic properties were seen between these very different distributions. Indeed, when the elastic properties were plotted against a value for the 'disorder' of the distribution in figure 4.10, no direct relationship was

found between the two. However, there does appear to be a minor effect, where in figure 5.2 the most random guides (zero, one, and four) appear to have higher elastic properties than the less random guides. There is no direct relationship with the level of disorder here though, only the general observation can be made that more disordered distributions of bonds often have somewhat higher elastic properties.

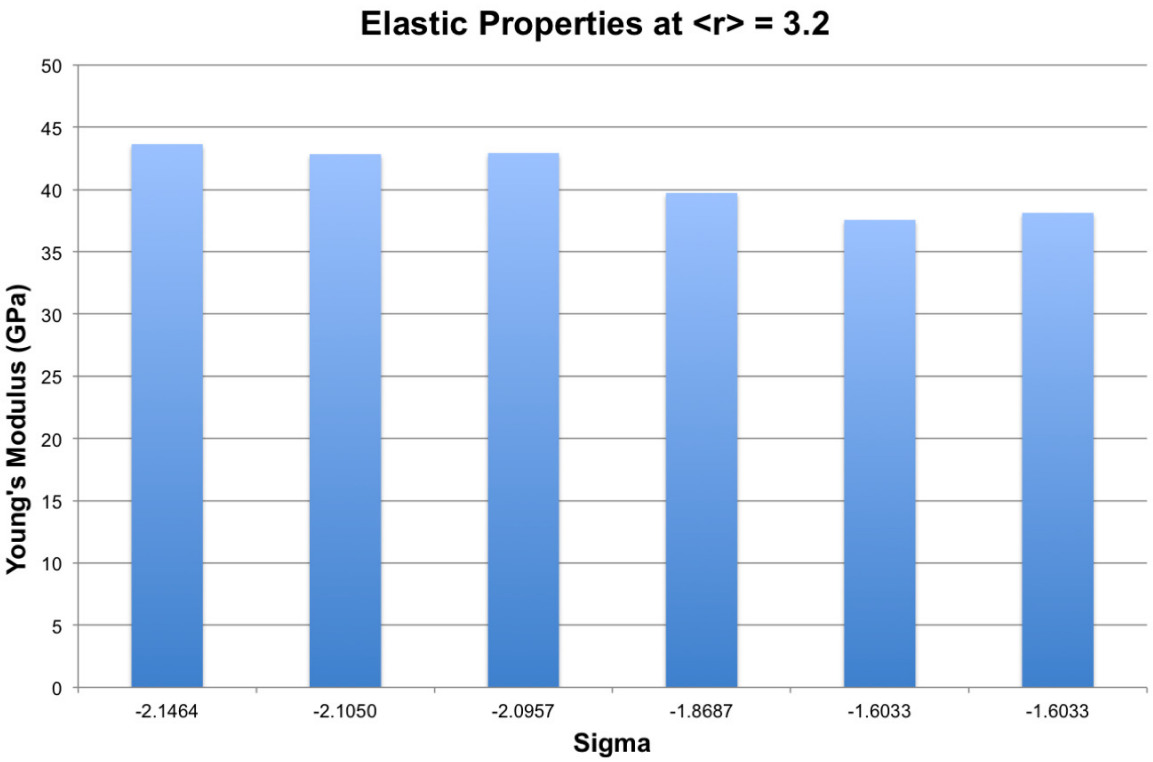

Figure 5.2: The Young's modulus at an average coordination of 3.2, for the different guides and random deletion. A more negative value of sigma corresponds to a higher level of disorder, as defined in equation 3.2.

5.3 Dependence of elastic properties on density

Figure 4.9 is one of the most compelling of this thesis. It shows a complete independence of elastic properties on the density in the system. A scattering of very different densities can be seen plotted across different average coordinations, with no effect on the overall elastic properties of the system. While in that figure only the Young's

modulus was plotted, there is no relationship between density and any other elastic property. The Makishima Mackenzie model relies on the density of the system to calculate the packing fraction of the system, in equation 2.34. The use of density appears to be another limitation of the model. As for why the model works despite this limitation, it is perhaps the case that in the narrow range of elastic coordinations present in most glasses, density works as a rough proxy to account for the variations in coordination, with more dense atoms generally having higher coordinations and vice versa.

5.4 Relative importance of three-body vs two-body potentials to elastic properties

Finally, to conclude the exploration of the MM model, this section will turn its attention from the packing density portion of the MM equation (2.32), and what that factor is omitting or mistakenly including, to the dissociation energy. This factor would seem to continue to make sense, even with an expanded understanding of the system: no longer a set of ionic balls, but now a set of Hookean springs. This dissociation energy would represent the strength of the springs. However, there does appear to be a limitation to using only dissociation energy, as this system relies on both the linear and angular Hookean springs to obtain the full elastic tensor, and only from that can good values be arrived at for experimental elastic properties. Indeed, Thorpe's percolation paper could only calculate c_{11} with only linear springs, while c_{12} is needed as well to find the Young's modulus. When the relative dependancy of the Young's modulus on the strength of both linear and angular springs in the system is plotted in figures 4.16 and 4.17, the system is found to be four times as sensitive to the angular bond strength as the linear bond strength. The bond dissociation energy does theoretically encompass all types of bonding interactions, but by being so all encompassing it does not acknowledge the relative importance of different bonding interactions. Replacing

it with two-body stretching and three-body bending bond energies would be an improvement. The bending bond energy contribution to the elastic properties would be weighed four times higher than the stretching bond energy contribution. Perhaps ab initio calculations could be designed to get such energy values.

5.5 Thorpe and Philips' Constraints Theory

Now a number of limitations and issues with the Makishima Mackenzie model have been outlined, based on the results of this study. The next question is then how do does one move forward with an understanding of these systems, beyond the ionic space filling ball metaphor of the Makishima Mackenzie model? The paper "Self-organization and the physics of glassy networks," published in the Philsophical Magazine in 2005 by Boolchand, Lucovsky, Phillips, and Thorpe, builds on the ideas outlined in Thorpe's Percolation paper (21). First, they bring up space filling models of network solids, and state that connectivity, omitted in space filling models, plays a very important role in actually understanding how such solids function. It has been demonstrated so far in this work the limits of space filling Makishima Mackenzie model, and this work shows the importance of connectivity to predicting the properties of the system, and fully understanding its mechanics.

Next, they study carefully the core differentiation established previously in rigidity percolation: between a floppy network and a rigid network. To do this, they explicitly define the number of degrees of freedom N_d and the number of constraints N_c in a system. The number of constraints is defined as the number of interatomic potentials, while the number of degrees of freedom is defined by the number of atoms. When $N_c < N_d$, the system is unconstrained and floppy; when $N_c > N_d$, the system is rigid and stressed. The former system would have zero elastic properties, while the latter would have non-zero elastic properties. However, there is an additional state, where $N_c = N_d$. Here the system is rigid, but unstressed. These different states are outlined

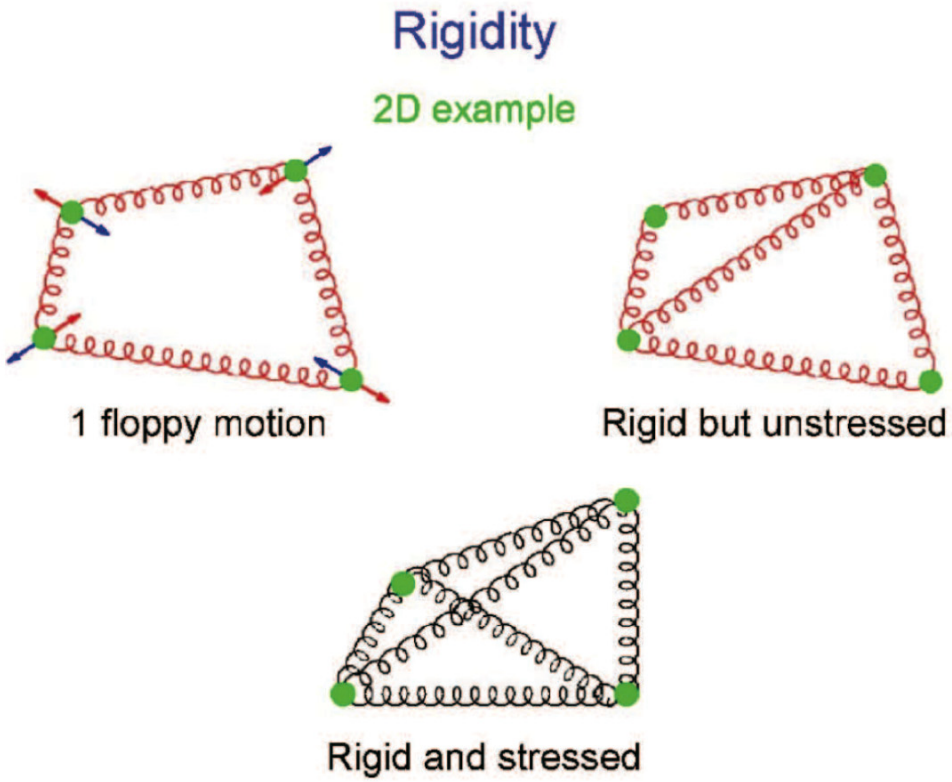

Figure 5.3: The three different states of a network solid outlined in a simple 2-D example. There are 8 degrees of freedom for 4 atoms, but three are translational and rotational. Each spring is one constraint. Figure reproduced from reference (21).

in figure 5.3.

Finally, they actually calculate the theoretical value of average coordination in a system with 'atomic' coordination centres and 'σ' and 'π' bonding links. The number of coordination centres defines the degrees of freedom of the system, while the two-body σ and three-body π links define the number of constraints of the system. They find the number of constraints equals the number of degrees of freedom at an average coordination of 2.39. This corresponds closely to the coordination number of borate glass, at 2.4, but is significantly below the coordination number of silicate glass, at 2.67.

Here there is another explanation for why the Makishima Mackenzie model appears to work well for silicate glass, but fails so badly for borate glass. For a rigid and stressed network system, as are all systems with coordinations above ~ 2.4, the space filling model of Makishima and Mackenzie works well enough at approximating the network. However, at coordinations near 2.4, the number of constraints in this system is near enough the number of degrees of freedom that the system is still rigid, but no longer stressed. This has the implication that such a system should have significantly lower elastic properties than a rigid and stressed system, but also elastic properties greater than the zero values in a floppy and unstressed system. This understanding of the properties of systems of different coordinations should hold for any system where the dominant constraints are two and three body nearest neighbour potentials. Indeed, the fact that 2.4 coordinate borate glasses have low but non-zero elastic properties, that higher coordinate systems have higher elastic properties, and that there do not appear to exist lower coordinate systems implies that the assumption of only two and three-body bonding forces is a good one for glassy networks.

The imposition of additional constraints on the system would change the coordination at which the system is rigid but unstressed. It should indeed be possible to predict the rigidity phase of the system based on an analysis of the most significant constraints present in the system. An interesting further case study would be phosphate glass, as for networking purposes phosphate oxide has a coordination of 2.4, but each phosphate centre has an additional double bonded terminal oxygen attached to it, imposing additional angular but not linear constraints on the system. This may explain why a system such as phosphate oxide, with low networking coordination, still has its properties well predicted by the space-filling Makishima Mackenzie model, which works for mostly higher coordinate systems. These questions would require further study.

5.6 Suggestions to improve model

So to this point a number of failings of the Makishima Mackenzie model have been outlined, a new theoretical framework for how to approach studying network glasses has been proposed, and explanations have been provided for why the Makishima Mackenzie model appears to work well in certain cases despite its simplifications. However, to move beyond the model, one must provide a mathematical formula that actually describes the dependence on the coordination of the system.

Focusing again on the Young's modulus, one sees that when average coordination is plotted in an exponential, the previous curve from figure 4.1 breaks into three discontinuous areas in figure **??**. These areas correspond to $\langle r \rangle \geqslant 2.52, 2.52 \geqslant \langle r \rangle \geqslant 2.4$, and $2.4 \geqslant \langle r \rangle$. These three regions would appear to correspond to the three different phases of rigidity available to a network system: $N_c > N_d$, $N_c = N_d$, and $N_c < N_d$. Any system with the same number of constraints per networking bond should have its general range of elastic properties predicted by what coordination range it falls into.

Figure **??** shows that for floppy systems with coordinations below 2.4, the Young's modulus is zero - only random fluctuations are present. For rigid systems with coordinations slightly above 2.4, the Young's modulus is non-zero, but small and largely independent of the coordination. For coordinations significantly above 2.4, there is a roughly exponential relationship between the Young's modulus and the coordination. One can define an equation that describes this last relationship:

$$E = C(e^{\langle r \rangle - 2.4} - 1), \tag{5.1}$$

where C is a constant that would include other physical properties of the system. One can further refine c, as it must include the bond energy of the system E_b, so $C = E_b * C*$. If good values are found for the bending and stretching bond energies,

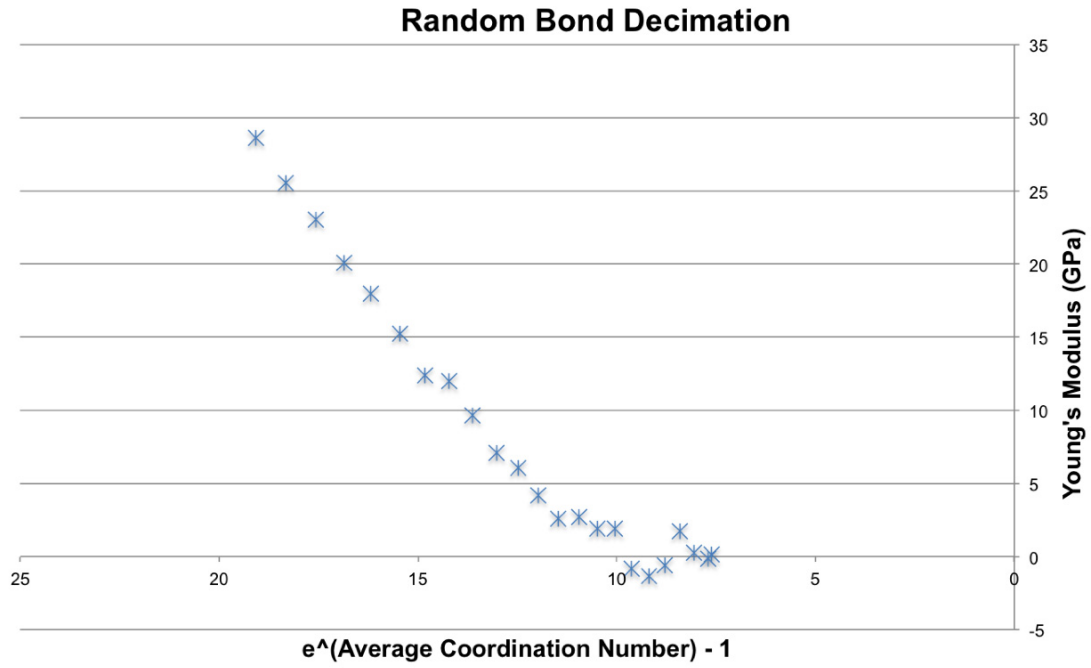

Figure 5.4: The Young's modulus from random deletions replotted with an exponential x axis. Coordinations from 3 to 2.1 are plotted.

E_b could be further refined: $E_b = 4E_{angular} + E_{linear}$. It is unclear what else beyond the bond energy may be included in C.

One can create similar plots (figures 5.5 and 5.6) for the bulk and shear moduli, showing this phase separation based on the average coordination number occurs for all elastic properties of the system. While the actual trends are different for each plot, the discontinuities in the lines occur at the same points.

To demonstrate that this new model makes comparable predictions to the MM model, calculation have been performed to predict the Young's modulus for the glass series 8-12, as presented in Makishima and Mackenzie's original paper (3). This is the series $(SiO_2)_{1-x}(Li_2O)_x$, where $x = 0.1, 0.15, 0.2, 0.25, 0.3$. For the calculation, the MM form $E = 2V_tG$ is used, equation 2.32, and V_t is replaced with the new coordination

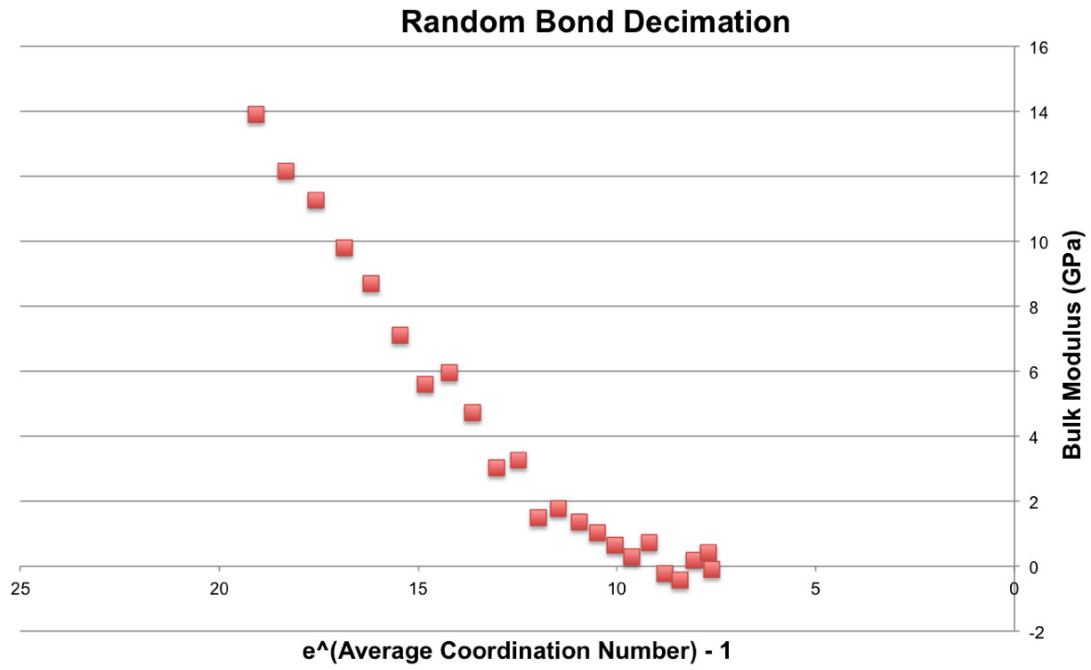

Figure 5.5: The Bulk modulus from random deletions replotted with an exponential x axis. Coordinations from 3 to 2.1 are plotted.

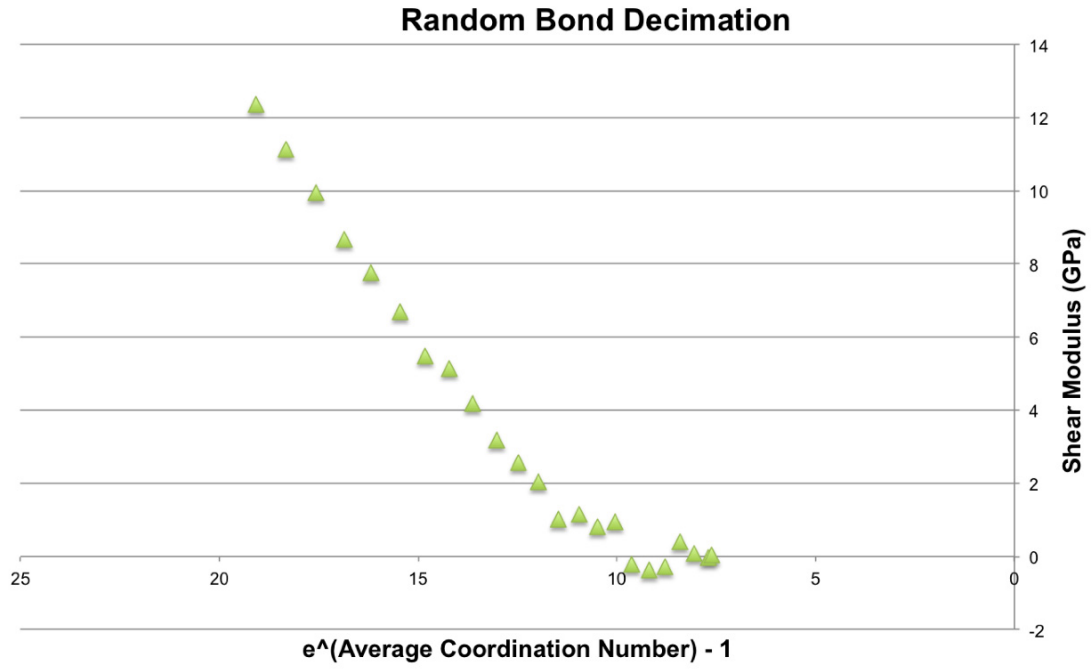

Figure 5.6: The Shear modulus from random deletions replotted with an exponential x axis. Coordinations from 3 to 2.1 are plotted.

factor. This gives the equation

$$E = 2G * (e^{\langle r \rangle - 2.4} - 1), \tag{5.2}$$

where $2G$ remains the same factor derived in the MM model. The results of this equation are plotted in the following table. Comparisons with experimental values and MM model values for the Young's modulus are also plotted.

Glass Number	x	Coordination Model	Experiment	Makishima Mackenzie
8	0.10	56.7 GPa	74.2 GPa	69.7 GPa
9	0.15	65.7 GPa	76.4 GPa	72.0 GPa
10	0.20	74.9 GPa	76.9 GPa	74.0 GPa
11	0.25	84.2 GPa	78.4 GPa	76.1 GPa
12	0.30	93.7 GPa	78.8 GPa	78.7 GPa

Table 5.1: Makishima Mackenzie Young's modulus vs experimental values vs coordination model for $(SiO_2)_{1\text{-}x}(Li_2O)_x$

One can see that the coordination model does follow the same trend that experimental calculations follow. It does not perform as well at predicting the rate of change across the series as the MM model does, and there are several possible reasons for this. First of all, for these calculations, the A constant in front of the coordination term (equation 5.1) was simply assumed to be $2G$, like in the MM model. This is likely missing important factors, and this approach requires further development. While a density term has been ruled out as a candidate, there is a possibility that a volumetric term would be present, as suggested by the Voronoi cell calculations. Another possible term could be a bonding density term (as distinct from an atomic density term). These could correct for the steep trend predicted by the coordination model. Secondly, it is important to understand how lithium interacts in this glass series. While these calculations assumed it is a 4 coordinate species, this may be not entirely accurate. Because lithium-oxygen bonds are so ionic in nature, a coordination based understanding of its bonding may overestimate the resistance of those bonds

to deformation. It may have a significantly lower effective coordination than 4, for constraint purposes.

The exploration of this question gets at the most interesting dichotomy between the Makishima Mackenzie model and a coordination based understanding of elasticity. Glass formers are generally covalent in bonding, which explains why the MM model's more ionic approach appears to fail, in particular for low coordinate systems like borate glasses. However, glass modifiers are often ionic in nature, which illustrates the limitations of the constraints based approach, and why the MM model is more effective at making predictions across a glass series. There appear to be two ways forward to resolve this dilemma: move forward with the constraints based approach, and determine an effective ionic correction to ionic bonding centres; or, hybridize the MM model's approach with the constraints based approach, using the MM model to calculate the effects of ionic glass modifiers, and the coordination based approach to calculate the starting elastic properties for the covalent glass formers.

Chapter 6

Conclusions

This work set out to answer a simple question: why does the Makishima Mackenzie model work for predicting the elastic properties of silicate and other glasses, yet fail so badly at predicting the properties of borate glasses. Thorpe's percolation paper inspired the exploration of this question, in particular the fact that in a system of springs, the elastic properties decreased to zero when the average coordination number of the system fell to 2.4 (19). The coincidence of this number to the actual experimental average coordination of pure boron oxide glass lead to the idea that the relationship between the coordination number of a system and its elastic properties should be further explored.

A model system was set up that was able to reproduce the experimental elastic properties for a silicon diamond lattice, and then bonds and atoms were randomly removed from it from it in a variety of ways, testing various properties of the system. To accomplish this, a sophisticated input generation program had to be implemented, one that allowed fine tuning of various aspects of the model. With the results of these calculations, the dependency of the elastic properties of the system to various parameters was explored. It was found that including both two and three-body potentials was critical to getting the elastic properties of the system correct, that there was a strong dependency of the elastic properties on the average coordination number of the system, and that the elastic properties were independent of the density of the system.

To further develop an understanding of how glasses behaved elastically, a theory of

rigidity 'phases' in network systems was used, outlined by Thorpe, Philips et al. in a paper from 2005 (21). This theory provided an understanding of how the relationship between average coordination and elastic properties changed at low coordinations. The key to this relationship was the relative numbers of constraints and degrees of freedom present in the network system, represented by the average coordination number of the system. Using this constraints based understanding of glassy systems, an explanation was developed for why the Makishima Mackenzie model fails for borate glasses, but still works for silicate glasses. A basis for improvement to the Makishima Mackenzie model was proposed that took the coordination number of the glass into account. Also, a method was proposed to determine whether a system could have its properties accurately predicted by the model, or whether its coordination was too low for that method to be effective.

To apply this new understanding of the relationship between elasticity and coordination, a system first considered in the original Makishima Mackenzie paper was examined (3). This examination found that the new equation could be applied to confirm the experimental trend, but it exaggerated the trend in its predictions. These results contrasted the strengths and weaknesses of the MM model and the coordination approach. This contrast suggests a pathway forward to synthesize these approaches for a model that better understands how elasticity arises in glass systems.

Bibliography

[1] R. E. Newnham, *Properties of Materials* (Oxford University Press, 2005).

[2] J. C. Mauro, C. S. Philip, D. J. Vaughn, and M. S. Pambianchi, International Journal of Applied Glass Science **5**, 2 (2014).

[3] A. Makishima and J. D. Mackenzie, Journal of Non-Crystalline Solids **12**, 35 (1973).

[4] J. Thorbahn, Local structure and the photoelastic response in zinc-modified oxide glass, Master's thesis, Dalhousie University, 2013.

[5] I. K.-H. Sun and M. L. Huggins, The Journal of Physical and Colloid Chemistry **51**, 438 (1947).

[6] A. Makishima and J. D. Mackenzie, Journal of Non-Crystalline Solids **17**, 147 (1975).

[7] T. Wei, Y. Hu, and L. Hwa, Journal of Non-Crystalline Solids **288**, 140 (2001).

[8] I. Hager, Journal of Materials Science **37**, 1309 (2002).

[9] Y. B. Saddeek and L. E. Latif, Physica B: Condensed Matter **348**, 475 (2004).

[10] Y. B. Saddeek, Journal of Alloys and Compounds **467**, 14 (2009).

[11] A. Makishima, Y. Tamura, and T. Sakaino, Journal of the American Ceramic Society **61**, 247 (1978).

[12] L. Huang and J. Kieffer, Physical Review B **74**, 224107 (2006).

[13] L. Huang, M. Durandurdu, and J. Kieffer, The Journal of Physical Chemistry C **111**, 13712 (2007).

[14] Y. B. Saddeek, Materials Chemistry and Physics **83**, 222 (2004).

[15] L. Hwa, T. Lee, and S. Szu, Materials Research Bulletin **39**, 33 (2004).

[16] R. Jindal, W. Jatmiko, I. V. Singh, and R. Jayaganthan, Journal of Minerals and Materials Characterization and Engineering **11**, 267 (2012).

[17] T. Rouxel, Journal of the American Ceramic Society **90**, 3019 (2007).

[18] S. Inaba, S. Fujino, and K. Morinaga, Journal of the American Ceramic Society **82**, 3501 (1999).

[19] M. Thorpe, Journal of Non-Crystalline Solids **76**, 109 (1985), Proceedings of the Workshop on Research Opportunities in Solids with Pulsed Neutrons Sources.

[20] S. Feng, M. F. Thorpe, and E. Garboczi, Physical Review B **31**, 276 (1985).

[21] P. Boolchand, G. Lucovsky, J. C. Phillips, and M. F. Thorpe, Philosophical Magazine **85**, 3823 (2005).

[22] H. Heinz, W. Paul, and K. Binder, Physical Review E **72**, 066704 (2005).

[23] W. Voigt, *Lehrbuch der kristallphysik (mit ausschluss der kristalloptik)*B.G. Teubners Sammlung von Lehrbüchern auf dem Gebiete der mathematischen Wissenschaften mit Einschluss ihrer Anwendungen (B. G. Teubner, 1928).

[24] A. Reuss, ZAMM - Journal of Applied Mathematics and Mechanics / Zeitschrift für Angewandte Mathematik und Mechanik **9**, 49 (1929).

[25] R. Hill, Proceedings of the Physical Society. Section A **65**, 349 (1952).

[26] Dracu-Teufel666, Ball of cubes and cube of balls, `http://dracu-teufel666.deviantart.com/art/Ball-of-cubes-and-cube-of-balls-289556652`, 2012.

[27] B. Bridge, N. D. Patel, and D. N. Waters, physica status solidi (a) **77**, 655 (1983).

[28] S. Plimpton, Journal of Computational Physics **117**, 1 (1995).

[29] F. H. Stillinger and T. A. Weber, Physical Review B **31**, 5262 (1985).

[30] Raincomplex, Voronoi diagram, `http://en.wikipedia.org/wiki/File:Euclidean_Voronoi_Diagram.png`, 2013.

[31] C. H. Rycroft, Voro++, `http://math.lbl.gov/voro++/`, 2008.

[32] J. C. Maxwell and W. D. Niven, **1**, 598 (2011).